The Canadian Mineralogist
Vol. 41, pp. 857-881 (2003)

CHLORINE ENRICHMENT AND HYDROUS ALTERATION OF THE SUDBURY BRECCIA HOSTING FOOTWALL Cu–Ni–PGE MINERALIZATION AT THE FRASER MINE, SUDBURY, ONTARIO, CANADA

JACOB J. HANLEY[§] AND JAMES E. MUNGALL

Department of Geology, University of Toronto, 22 Russell Street, Toronto, Ontario M5S 3B1, Canada

ABSTRACT

An assemblage of hydrous, Cl-bearing alteration-induced minerals is present within 150 m of footwall-style Cu–Ni–PGE sulfide mineralization hosted by the Sudbury Breccia at the Fraser Copper zone, Fraser mine, Onaping–Levack area, Ontario. The pyroxene hornfels to hornblende hornfels contact-metamorphic aureole of the Sudbury Igneous Complex (SIC) contains less than 15 modal % hydroxysilicates. Near the mineralized areas, a diagnostic assemblage of secondary minerals of the albite–epidote hornfels facies is present in the matrix of the Sudbury Breccia; it contains 25 to 80% actinolite + chamosite as well as epidote + sodic plagioclase ($An_{2.8–42}$) + quartz ± titaniferous magnetite ± biotite ± K-feldspar ± titanite. The Cl content and Cl/(Cl + F) values of amphibole and biotite in this matrix are elevated within 150 m of mineralization, and increase toward known occurrences of sulfides. Parameters of K, Na, and *A*-site occupancy correlate with Cl content in actinolite in such matrix material. The value of Mg# is lower in biotite in the matrix near mineralized areas and is inversely correlated with Cl/(Cl + F) in the biotite, reflecting Mg–Cl or Fe–F avoidance. Calculated temperatures of amphibole–plagioclase equilibration for the diagnostic hydrous assemblage are between 442 to 540 ± 75°C. The assemblage formed during a retrograde metamorphic event during or after footwall Cu–Ni–PGE mineralization, and after passage of peak conditions of contact metamorphism at the base of the SIC. The enrichment of Cl in this assemblage was the result of the increased amounts of free Cl relative to F in the equilibrating fluid, and favorable cation proportions for incorporation of Cl into the structure of hydroxysilicate minerals. The Cl-bearing assemblage accounts for a significant portion of the bulk halogen content of Sudbury Breccia matrix. It is unique to zones of Sudbury Breccia that host mineralization, and hence may be used to identify prospective areas.

Keywords: halogens, Cu–Ni–PGE mineralization, Sudbury Breccia, metamorphism, amphibole, biotite, pseudotachylite, retrograde effects, alteration, Sudbury, Ontario.

SOMMAIRE

Nous décrivons un assemblage de minéraux d'altération hydratés et contenant du chlore dans une auréole de 150 m autour des indices minéralisés (Cu–Ni–EGP, sulfures) dans le socle bréchifié sous le complexe igné de Sudbury, à la zone dite de Fraser Copper, exploitée à la mine Fraser, région de Onaping–Levack, en Ontario. Les hornfels à pyroxène et à hornblende de l'auréole de contact autour de ce complexe contiennent moins de 15% de ces silicates hydroxylés. Près des indices imnéralisés, en revanche, nous trouvons un assemblage distinctif de minéraux secondaires équilibrés dans le faciès des hornfels à albite–épidote, développés dans la matrice de la Brèche de Sudbury; sont présents de 25 à 80% d'un assemblage à actinolite + chamosite, de même que épidote + plagioclase sodique ($An_{2.8–42}$) + quartz ± magnétite titanifère ± biotite ± feldspath potassique ± titanite. La teneur en Cl et les valeurs du rapport Cl/(Cl + F) de l'amphibole et de la biotite dans cette matrice sont élevées à l'intérieur de cette auréole de 150 m autour des zones minéralisées, et augmentent dans la direction de l'enrichissement en sulfures. Les paramètres K, Na, et l'occupation du site *A* montrent une corrélation avec la teneur en Cl de l'actinolite de la matrice. La valeur de Mg# est plus faible dans la biotite de la matrice près des zones minéralisées, et montre une corrélation inverse avec Cl/(Cl + F) de la biotite, ce qui témoigne de l'instabilité des agencements Mg–Cl et Fe–F. Les températures calculées de l'équilibre entre amphibole et plagioclase de cet assemblage hydraté sont entre 442 et 540°C ± 75°C. L'assemblage distinctif de minéraux d'altération se serait formé au cours d'un événement de métamorphisme rétrograde, pendant ou suivant la minéralisation du socle, après le paroxysme du métamorphisme de contact à la base du complexe de Sudbury. L'enrichissement en Cl de l'assemblage était le résultat de la disponibilité accrue du Cl par rapport au F dans la phase fluide en circulation, et d'une combinaison favorable des cations pour l'incorporation du Cl dans la structure des minéraux hydroxylés. Ces phases minérales expliquent une bonne partie du bilan des halogènes dans la matrice de la Brèche de Sudbury. Elles semblent uniquement développées dans les zones de la Brèche qui renferment des zones minéralisées. On peut donc s'en servir comme indicateur de minéralisation.

(Traduit par la Rédaction)

Mots-clés: halogènes, minéralisation Cu–Ni–EGP, Brèche de Sudbury, métamorphisme, amphibole, biotite, pseudotachylite, effets rétrogrades, altération, Sudbury, Ontario.

§ *E-mail address*: hanley@geology.utoronto.ca

Introduction

Determination of the halogen contents of igneous and metamorphic rocks and common rock-forming hydroxysilicate minerals such as amphiboles, micas, and apatite can provide insight into the composition and evolution of fluids involved in hydrothermal, magmatic, and metamorphic processes (Munoz & Ludington 1977, Boudreau *et al.* 1986a, b, Zhu & Sverjensky 1991, 1992, among others). The proportion of cations in these minerals, temperature of formation, fluid composition, and post-crystallization leaching are the principal controls on the total content of halogens and their relative abundance in hydroxysilicates (Ramberg 1952, Rosenberg & Foit 1977, Munoz 1984, Volfinger *et al.* 1985, Morrison 1991, Zhu & Sverjensky 1991, 1992, Oberti *et al.* 1993, and others therein).

In this study, we examine the distribution and composition of halogen-bearing minerals in the fine-grained matrix of a rock type known as the Sudbury Breccia, exposed near the contact of the Sudbury Igneous Complex (SIC). We focus on this rock type, as it comprises up to 80 vol. % of the host rocks to the footwall Cu–Ni–PGE (platinum-group element) sulfide ores of the Sudbury structure and is a significant host-rock to other footwall-type ores in the Sudbury district (*e.g.,* the Thayer Lindsley deposit; Binney *et al.* 1994). We provide a mineralogical and mineral-chemical description of a halogen-bearing hydroxysilicate assemblage in the matrix of the Sudbury Breccia that is diagnostic of proximity to footwall-type Cu–Ni–PGE sulfides, and discuss possible mechanisms of formation for the assemblage in relation to deposition of Cu–Ni–PGE sulfide ore in the footwall.

Background

Geological setting and location of study

The Fraser mine is located at the northern margin of the Sudbury Igneous Complex, approximately 60 km north of the city of Sudbury, in Ontario. Contact-style Ni–Cu–PGE and footwall-style Cu–Ni–PGE deposits at the Fraser mine occur along the northwestern edge of the SIC (Fig. 1a). The SIC is a Proterozoic igneous body considered to be the product of a meteorite impact at 1850 Ma (Dietz 1964, Krogh *et al.* 1984, Grieve 1994). In the vicinity of the Fraser mine, the SIC forms a tabular sheet dipping to the southeast, comprising noritic to gabbroic cumulates overlain by a granophyric residuum. Along the basal contact of the SIC, partially melted target rocks comprise an igneous-textured footwall breccia (locally called "late granite breccia"). At the Fraser mine, the footwall breccia overlies Archean gneiss, granite, migmatite, and diabase dykes of the Superior Province. The cooling of the SIC resulted in a zoned contact-metamorphic aureole (albite–epidote hornfels to pyroxene hornfels in grade) extending about 1 km be-

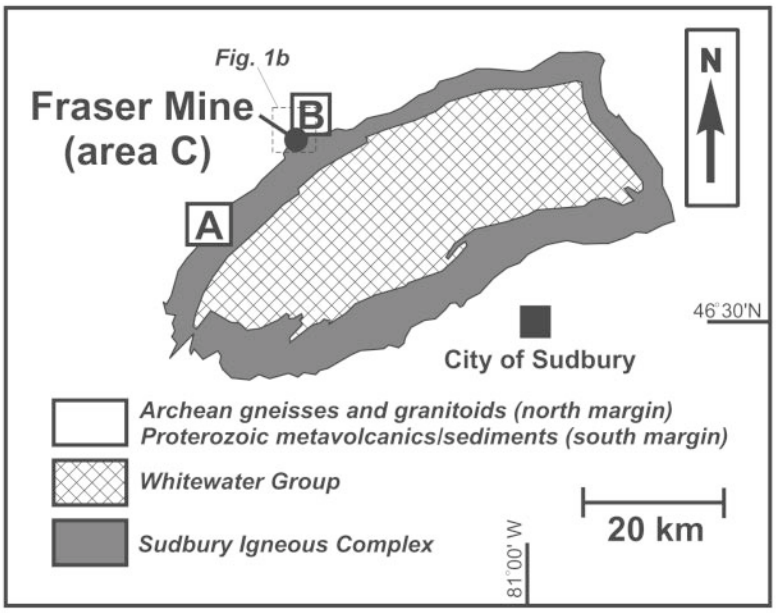

FIG. 1a. Generalized geological map of the Sudbury Igneous Complex (SIC) showing the location of the Sudbury Breccia, and study areas A through C. The area in the dashed box is shown in detail in Figure 1b.

low the base of the SIC into the Archean host-rocks (Coats & Snajdr 1984, Dressler 1984, Farrow 1995).

During impact, the excavation, brecciation, and melting of the footwall rocks prepared structural traps along the basal contact of the SIC, in which contact-style Ni–Cu–PGE sulfide mineralization was introduced during the differentiation of the SIC. Magmatic differentiation of sulfide liquid along the lower contact of the SIC resulted in the formation of residual sulfide liquid enriched in Cu, Pt, Pd and Au. This Cu-rich sulfide liquid then settled into zones of brecciated gneissic rock (Sudbury Breccia) in the footwall to the SIC (*i.e.*, Li 1992, Li & Naldrett 1993, Morrison *et al.* 1994). The zones of Sudbury Breccia that host footwall-style Cu–Ni–PGE mineralization occur below the Strathcona embayment, subparallel to the embayment axis, which plunges approximately 21° SSW (Fedorowich *et al.* 1999) (Fig. 1b).

Multiple hydrothermal events remobilized and reconcentrated some of the base metals, Au, Ag, and PGE (*e.g.*, Farrow 1995, Farrow & Watkinson 1992, Marshall *et al.* 1999, Molnar *et al.* 2001).

Characteristics of the Sudbury (*Levack*) *Breccia*

The Sudbury Breccia is one of several types of breccia associated with the Sudbury structure. The matrix of the Sudbury Breccia is composed of pseudotachylite (Dressler 1984); it resembles pseudotachylite identified at its type locality in the Vredefort impact structure in South Africa (Shand 1916, Wilshire 1971). Pseudotachylite was originally named for its resemblance to

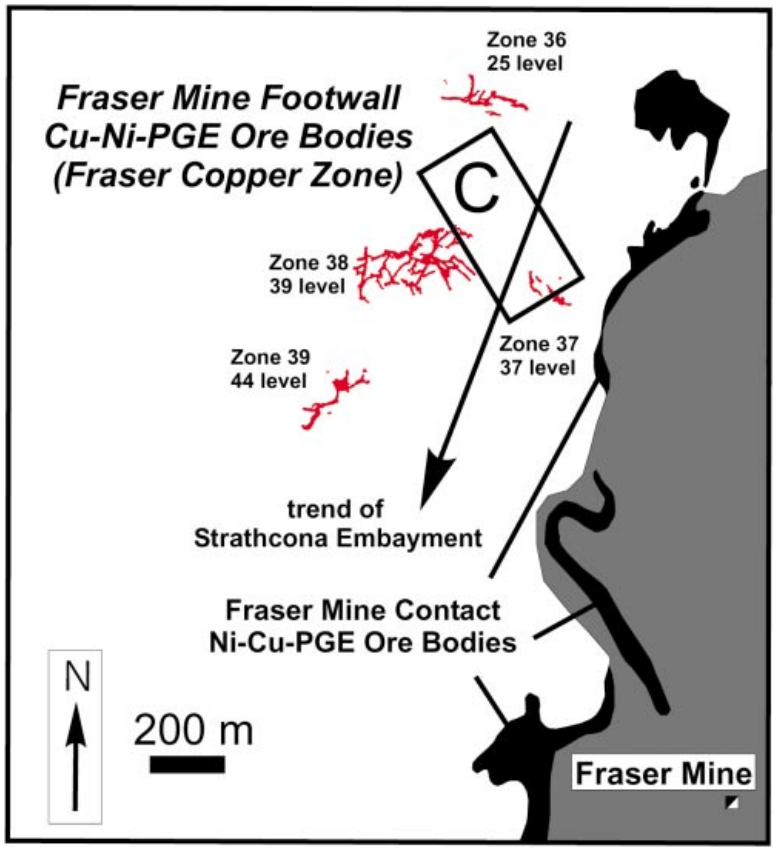

FIG. 1b. Plan view of the Fraser mine orebodies projected to the 2500 foot level. Note that the SIC has been greatly simplified to include the footwall or "late granite" breccia. Contact-style Ni–Cu–PGE orebodies are shown in black. Representative cross-cuts for the four footwall-style Cu–Ni–PGE ore zones (Zones 36–39, shown in red in the electronic version) and lie beneath the Strathcona Embayment, which trends to the SSW, plunging approximately 21°. Study area C includes footwall Cu–Ni–PGE sulfide veins in Zone 37 and Zone 38.

tachylite, which is a black, glassy rock formed on the edges of basaltic intrusions. Pseudotachylite is formed as a result of seismogenic faulting or, at Sudbury and at the type locality in the Vredefort structure, from faulting due to meteorite impact (Spray 1997). The pseudotachylite matrix is preserved as very fine-grained to aphanitic, diabasic-textured to equigranular material reflecting its probable origin by frictional melting of wallrocks. The matrix encloses angular to rounded clasts of local host-rocks. The greatest volumes of Sudbury Breccia are found surrounding and along the surfaces of the structurally complex depressions of the footwall contact beneath the SIC known as embayments, hosting the sulfide mineralization described above (Cowan 1968, Morrison *et al.* 1994, Fedorowich *et al.* 1999). The common occurrence of footwall mineralization within zones of Sudbury Breccia indicates that the breccia bodies served as conduits in the migration of sulfide liquid or metal-bearing hydrothermal fluid (Morrison *et al.* 1994, Farrow 1995).

Review of previous work

At Sudbury, several investigators have examined the halogen budget and the origin of assemblages of alteration minerals associated with footwall-style Cu–Ni–PGE and contact-style Ni–Cu–PGE ores (Springer 1989, Farrow & Watkinson 1992, Li 1992, Li & Naldrett 1993, Jago *et al.* 1994, Farrow 1995, McCormick & McDonald 1999, Marshall *et al.* 1999, Kormos 1999, Molnar *et al.* 2001, McCormick *et al.* 2002). These investigators have documented alteration assemblages of Cl-rich phases containing up to several wt.% Cl, including ferropyrosmalite, annite, ferro-actinolite, ferrohornblende, hastingsite, tschermakite, and Cl-poor phases (less than 0.18 wt.% Cl), including actinolite and magnesiohornblende, occurring along sulfide – host-rock contacts and in host rocks within a few meters of mineralization. The formation of the Cl-poor and Cl-rich alteration assemblages is considered to be the product of at least two major hydrothermal events related to ore deposition: an early, high-temperature event, contemporaneous with sulfide emplacement involving a Cl-poor fluid, and a late, low-temperature event involving a Cl-rich hybrid fluid derived from mixing of an exsolved fluid (from the SIC or cooling sulfide ores) with local groundwaters (McCormick & McDonald 1999, Marshall *et al.* 1999). Recently, McCormick *et al.* (2002) recognized the presence of a broad geochemical halo (hundreds of meters in scale) enriched in Cl relative to F, and Na relative to K, surrounding contact-style Ni–Cu–PGE mineralization hosted in footwall breccia and norite in the Strathcona Embayment.

Below the SIC contact, anomalous bulk-rock concentrations of Cl and F were reported in Sudbury Breccia up to 50 m from footwall Cu–Ni–PGE ore at the McCreedy East mine (Jago *et al.* 1994) and the Fraser Copper zone (Kormos 1999). Hanley (2002) found anomalous bulk-rock concentrations of Cl and Br in the Sudbury Breccia at distances of up to 150 m from mineralization in the Fraser Copper zone. Alteration assemblages genetically associated with footwall Cu–Ni–PGE mineralization were previously reported as restricted only to weakly mineralized host-rocks occurring within a few meters of massive sulfide veins (*e.g.*, Farrow 1995).

Sampling and Classification of Samples of Sudbury Breccia Matrix

Samples of matrix of the Sudbury Breccia from the footwall environment were collected in three areas (Fig. 1a) along the margin of the SIC. Area A (Fig. 2a) comprises representative barren outcrops of Sudbury Breccia, found at least 1 km from known orebodies or sites of reported footwall Cu–Ni–PGE mineralization, along a 4 × 12 km segment of the northwestern margin of the SIC. Area B (Fig. 2b) comprises mineralized and barren outcrops of Sudbury Breccia northeast of the Fraser mine; it includes the up-plunge, subeconomic surface-exposure of footwall sulfide ores found in the Fraser mine. Area C (Fig. 2c) is located in stope #1620 of Zone 38 and along a haulage drift connecting Zone 38 and Zone 37 in the Fraser Copper zone, Fraser mine (3700-foot level).

Samples collected from each of the study areas were classified according to their proximity to known foot-

FIG. 2. Plan maps of study areas showing observed zones (colored areas) and inferred boundaries (dashed lines) of the normal contact-metamorphic aureole, and hydrous retrograde alteration-induced assemblages indicative of proximity to mineralization. Observed zones are based on detailed petrography of Sudbury Breccia matrix samples, and colored areas correspond to the observed metamorphic or alteration-induced assemblages of minerals (see legend). Mineral abbreviations: pl plagioclase, qtz quartz, ep epidote, act actinolite, hbl hornblende, bt biotite, cpx pyroxene, chm chamosite, mgt titaniferous magnetite, kfs K-feldspar, ttn titanite. Sample sites (distal: black squares, peripheral: grey triangles, proximal: white circles) for electron-microprobe analysis of halogen-bearing minerals are labeled. a. Study area A (northwestern margin of SIC) showing the typical zoned hornfels aureole (simplified) around the SIC. b. Study area B (up-plunge surface exposure of footwall Cu–Ni–PGE mineralization) showing the observed extent of the diagnostic retrograde (ab–ep hornfels) assemblage that replaced or overprinted the earlier, contact-metamorphic cpx hornfels assemblage. The inferred positions of the normal contact-metamorphic zone boundaries (cpx hornfels to hbl hornfels, and hbl hornfels to ab–ep hornfels) also are shown. c. Study area C (Fraser Copper zone) projected to the 3700 foot level showing simplified mine geology of Zones 37 and 38. The ore-hosting

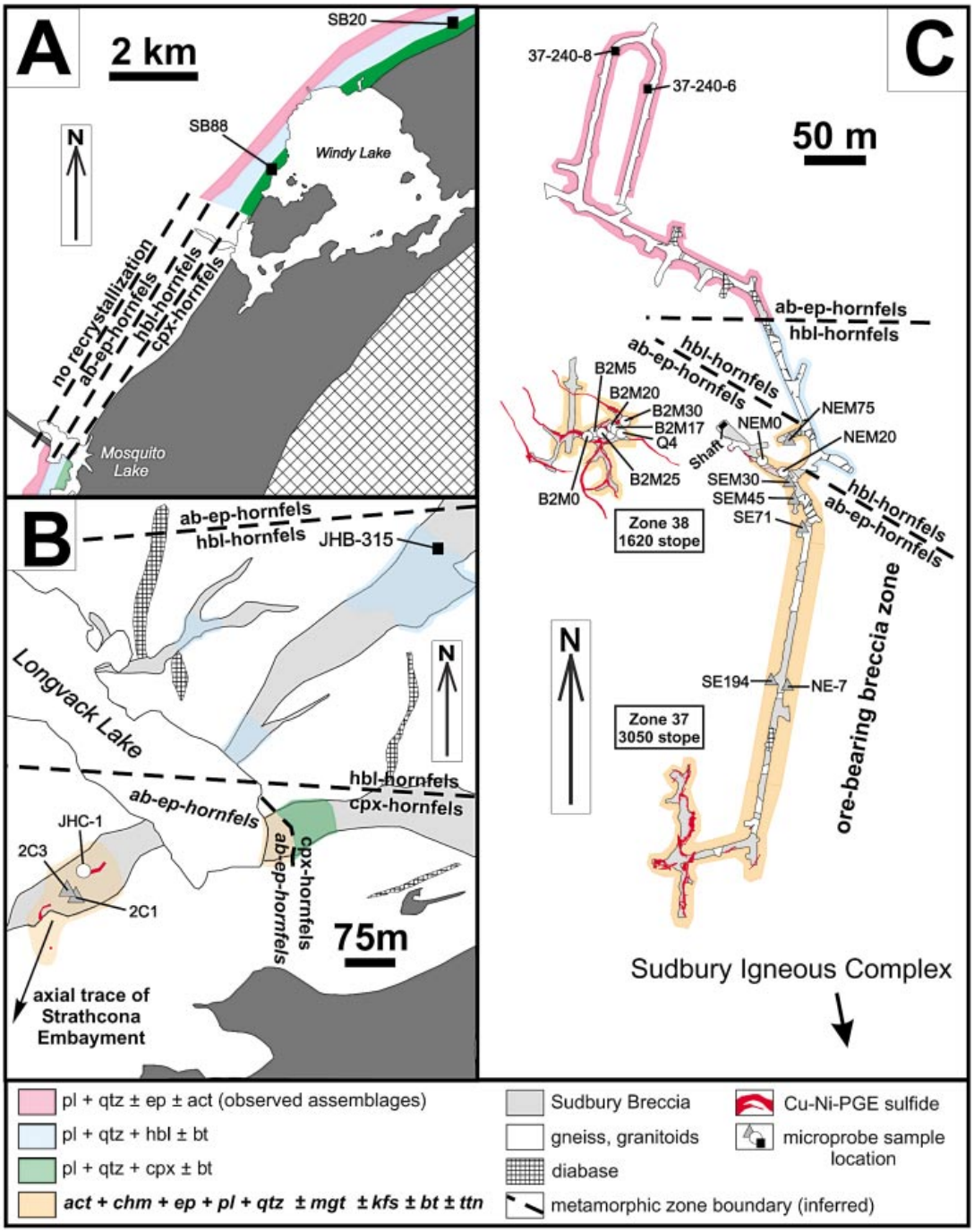

breccia zone is comprised of 46 vol.% brecciated gneissic rocks. Sudbury Breccia abundance decreases to less than 18% in the footwall of Zone 38 (northeast of Zone 38). The diagnostic retrograde (ab–ep hornfels) assemblage replaced rocks of hbl hornfels grade. The northeastern extent of this replacement is the boundary of the ore-hosting breccia zone where the transition from retrograde ab–ep hornfels to contact-metamorphic hbl hornfels was observed. The position of the contact-metamorphic zone boundary for the normal transition between hbl hornfels and ab–ep hornfels also is shown.

wall sulfide mineralization, and occurrence either within or outside of a Sudbury Breccia zone known to host mineralization. Mineralization is defined here as the occurrence of veinlets or large (mm- to cm-scale) blebs of chalcopyrite ± cubanite ± millerite in Sudbury Breccia matrix or in gneissic clasts, that may be recognized easily in hand sample. A Sudbury Breccia zone is defined as a thick, structurally continuous lens or body of Sudbury Breccia that may host mineralization. These may be recognized by a high volumetric abundance (averaging 40 vol.%) of matrix and clast material relative to unbrecciated or weakly brecciated rock. For example, in the Fraser Copper zone, ore zones 37 and 38 are hosted in a zone approximately 200 m wide of Sudbury Breccia that consists of approximately 46 vol.% Sudbury Breccia (matrix + clasts) (Fig. 2c), whereas the adjacent hanging-wall of this Sudbury Breccia zone is weakly brecciated and contains less than 18 vol.% matrix and clasts (Fedorowich *et al.* 1999). The limits of this breccia zone to the east of the haulage drift between Zones 38 and 37 and in the hanging wall of Zone 38 are unknown owing to limited data derived from drilling in that area.

Three sample divisions were used: distal breccia matrix was sampled beyond the mineralization-hosting breccia zones, at distances greater than 150 m from known Cu–Ni–PGE mineralization; peripheral breccia matrix was sampled within the mineralization-hosting breccia zones at distances of 10 to 150 m from mineralization, and proximal breccia matrix was sampled within the mineralization-hosting breccia zones at distances of less than 10 m from mineralization. Because of the erratic distribution of Sudbury Breccia, its limited exposure underground, and the difficulty in modeling zones of Sudbury Breccia in three dimensions from the limited data available, it was not possible to obtain samples known to originate further than 150 m away from mineralization and yet in the same, structurally continuous zone of ore-hosting breccia. The mineralogical characteristics of matrix samples classified as distal should be considered as being representative of background conditions unrelated to footwall-style Cu–Ni–PGE mineralization.

Field and Petrographic Observations of Contact Metamorphism in Barren Sudbury Breccia

Through our examination of several hundred thin sections of Sudbury Breccia matrix from localities distal to known occurrences of mineralization, we have confirmed the presence of a zoned contact-metamorphic aureole extending at least 1 km below the base of the SIC (Coats & Snajdr 1984, Dressler 1984, Farrow 1995). Figures 3a and 3b illustrate unrecrystallized (2 km from the SIC) and contact-metamorphosed Sudbury Breccia (150 m from the SIC contact).

In general, the appearance of the first contact-metamorphic features in Sudbury Breccia matrix is abrupt, occurring over a 100-m interval approximately 1300 m from the contact. The overall grain-size of the Sudbury Breccia matrix increases with increasing proximity to the SIC contact. The maximum grain-size observed (at a distance of approximately 50 to 100 m from the contact) for feldspar and quartz is between 100 and 400 μm. Small lithic clasts within the matrix show progressive recrystallization into granoblastic patches with little or no mafic mineral content, ultimately being replaced by patches and veinlets of massive quartz and granophyre (intergrown quartz + K-feldspar). The mineral assemblage of the pseudotachylite matrix is generally consistent with the zoned contact-metamorphic aureole described by Dressler (1984) and Coats & Snajdr (1984), falling into the following facies divisions: albite–epidote hornfels (plagioclase + quartz ± epidote ± actinolite) occurring 1300 to 600 m from the contact, hornblende hornfels (plagioclase + quartz + hornblende ± biotite) occurring 600 to 350 m, and pyroxene hornfels (plagioclase + quartz + pyroxene ± biotite) occurring within 350 m of the basal contact of the SIC (Fig. 2a).

The occurrence of a granophyric intergrowth of K-feldspar and quartz, optically continuous patches of "flood" quartz, and the growth of biotite and amphibole within Sudbury Breccia matrix were previously noted by Morrison *et al.* (1994) as a characteristic of intensely metamorphosed Sudbury Breccia nearest to the inferred conduits of fluid in footwall ore-zones. In their opinion, the development of these features is an indication of ore proximity; however, we report these features to be common to Sudbury Breccia matrix in locations several kilometers away from footwall mineralization throughout much of the footwall environment. Contact-metamorphic effects evidently were not confined to footwall ore-zones.

Field and Petrographic Observations of Retrograde Alteration in Mineralized Sudbury Breccia

The primary contact-metamorphic assemblages of the Sudbury Breccia matrix from proximal and peripheral sites (*i.e.*, within 150 m of mineralization) have been intensely altered to a hydrous secondary assemblage. This assemblage, which we believe to be diagnostic of proximity to mineralization, consists of (in decreasing abundance): amphibole (specifically, actinolite) + chlorite (specifically, chamosite) + epidote + sodic plagioclase ($An_{2.8–42}$) + quartz ± titaniferous magnetite ± K-feldspar ± biotite ± titanite. Several samples of peripheral Sudbury Breccia matrix were used to determine, by petrographic examination of mineral-replacement textures, a possible paragenetic sequence and a series of relevant hydration-type reactions that describe the

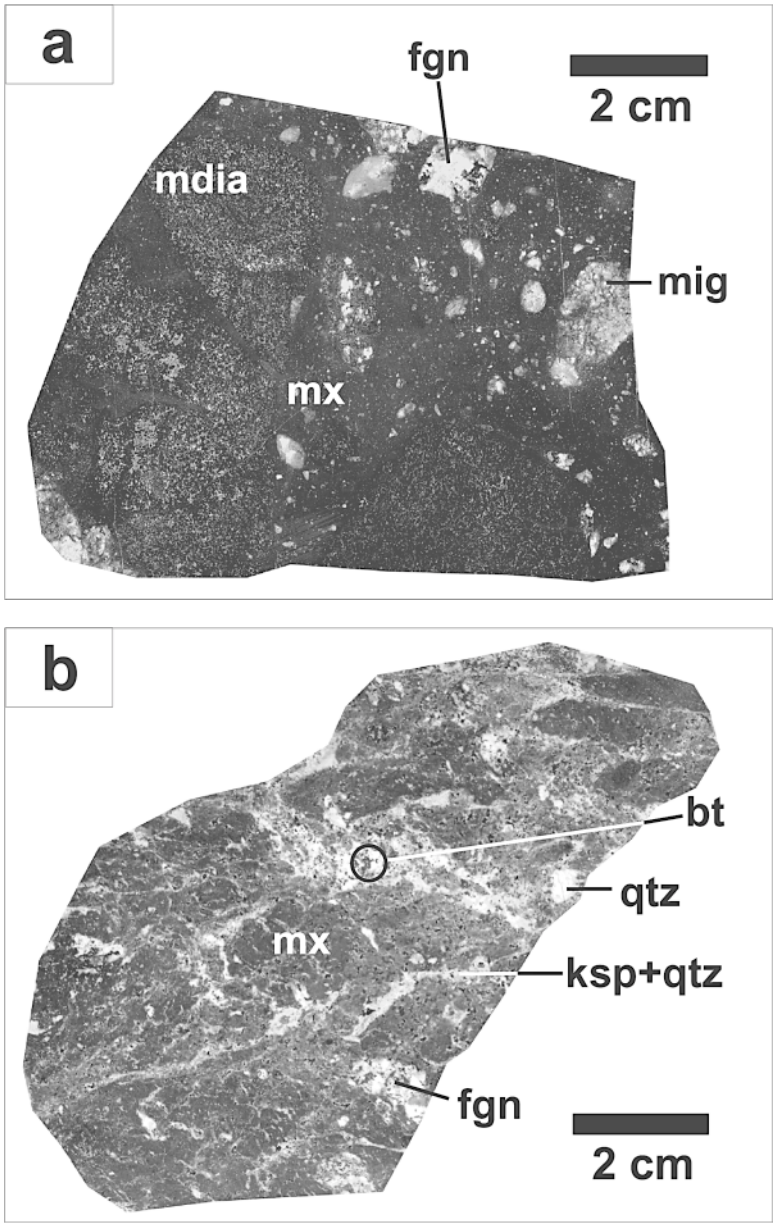

FIG. 3. Sudbury Breccia in hand specimen. a. Typical fresh, unrecrystallized breccia sampled 2 km from the SIC contact. Clasts of felsic gneiss (fgn), migmatite (mig), and diabase (mdia) are hosted in an aphanitic, black matrix (mx). b. Typical contact-metamorphosed breccia from a distance of 150 m from the SIC contact. Veinlets of K-feldspar and quartz (ksp + qtz), large patches of optically continuous quartz (qtz), and biotite poikiloblasts (bt) are visible. Clasts of felsic gneiss (fgn) and matrix (mx) have totally recrystallized.

formation of the diagnostic assemblage from the former contact-metamorphic assemblages. Figures 4a to 4d demonstrate the development of the principal mineral components of the diagnostic assemblage. In rocks previously of pyroxene hornfels grade (Fig. 4a), plagioclase and pyroxene were replaced by epidote and actinolite, with actinolite pseudomorphs after pyroxene dominating the assemblage (Fig. 4b). The following hydration-type reaction is proposed:

$$9\ CaAl_2Si_2O_8 + 5\ Ca(Mg, Fe)Si_2O_6 + 4\ H_2O =$$
anorthite diopside fluid

$$Ca_2(Mg,Fe)_5Si_8O_{22}(OH)_2 + 6\ Ca_2Al_3Si_3O_{12}(OH)$$
actinolite–tremolite epidote

$$+ 2\ SiO_2$$
quartz

Diopside was consumed completely, as there is no pyroxene preserved in the diagnostic assemblage. The formation of epidote consumed some plagioclase; however, plagioclase must have persisted in the presence of epidote for the following reaction to occur, representing the first appearance of a chlorite-group mineral (Fig. 4b):

$$14\ CaAl_2Si_2O_8 + 2\ Ca_2(Mg,Fe)_5Si_8O_{22}(OH)_2$$
anorthite actinolite–tremolite

$$+ 11\ H_2O =$$
fluid

$$8\ Ca_2Al_3Si_3O_{12}(OH) + (Fe,Mg)_{10}Si_6Al_4O_{20}(OH)_{16}$$
epidote chamosite

$$+ SiO_2$$
quartz

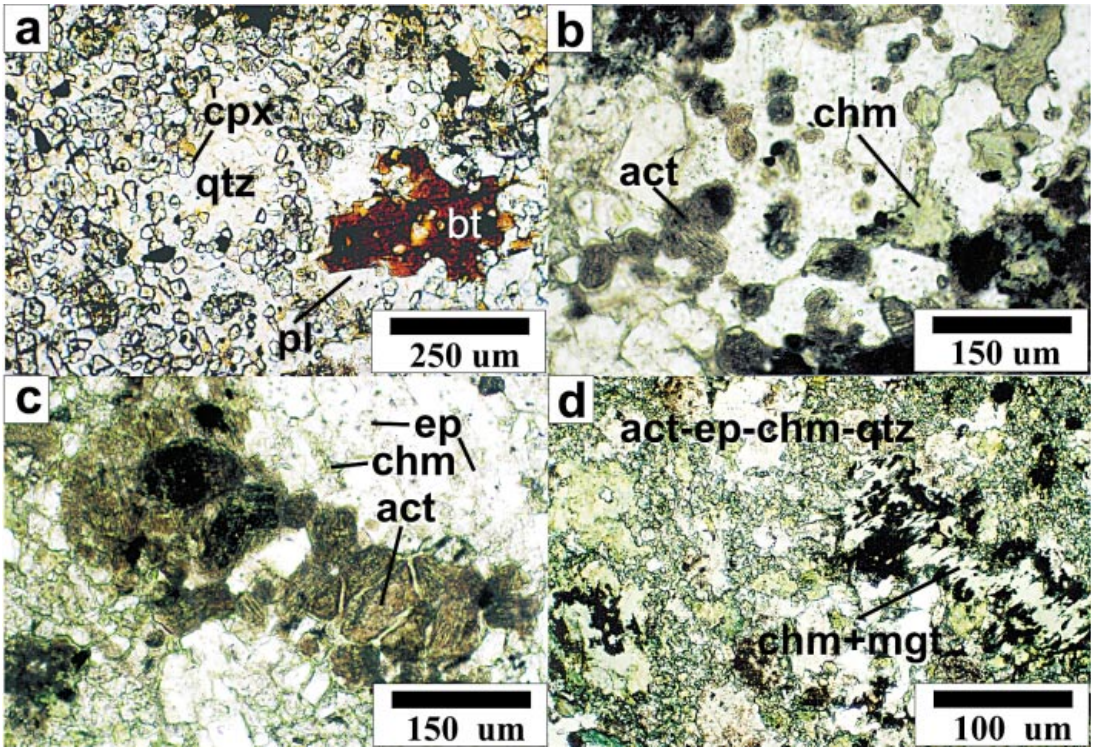

FIG. 4. Photomicrographs (plane-polarized light) of Sudbury Breccia matrix showing the development of the diagnostic retrograde assemblage. a. Typical contact-metamorphic assemblage from a distal site (SB88) showing pyroxene hornfels grade. Poikiloblastic biotite (bt) enclosing quartz (qtz) and plagioclase (pl). Fresh, tabular clinopyroxene (cpx) grains are hosted in a matrix of quartz and plagioclase. b. Pyroxene is first replaced by type-II amphibole (act) and mantled in epidote (lower left of image). Type-II amphibole is then replaced by chamosite (chm) (right side of image). c. Pyroxene replaced by type-II amphibole (act) and partly replaced or mantled by chamosite (chm). Granular epidote (ep) is visible in the groundmass (upper right of image) . The growth of chamosite is not restricted to regions where type-II amphibole exist, but also occurs along grain boundaries in the quartz and plagioclase groundmass, resulting in the development of a dense, interconnected mesh of hydroxysilicate mineral grains. d. Typical diagnostic retrograde assemblage from a peripheral site (NE–7) showing the major component mineral phases of the assemblage. A large pseudomorph of chamosite (chm) + titaniferous magnetite (mgt) (after biotite) sits in a groundmass of actinolite (act) + epidote (ep) + chamosite (chm) + quartz (qtz). Modal abundance of hydroxysilicate minerals (act + ep + chm) = 50 vol.%.

As this reaction proceeded and the assemblage recrystallized, a dense intergrowth of actinolite, epidote, chlorite, and quartz resulted (Figs. 4c, d), with a large amount of plagioclase having been consumed. In many samples, plagioclase was absent from the assemblage, having been totally consumed during the production of chlorite.

Similarly, in rocks previously at hornblende hornfels grade, the hydration of hornblende produced epidote + actinolite + chlorite in a single reaction (Fig. 5a):

$$25\ Ca_2(Mg,Fe)_3\ Al_3Si_6O_{22}(OH)_2 + 44\ H_2O =$$
hornblende — fluid

$$Ca_2(Mg, Fe)_5\ Si_8O_{22}(OH)_2$$
actinolite–tremolite
$$+ 7\ (Fe,Mg)_{10}Si_6Al_4O_{20}(OH)_{16}$$
chamosite

$$+ 24\ Ca_2Al_3Si_3O_{12}(OH) + 28\ SiO_2$$
epidote — quartz

In each of these reactions, large amounts of quartz are produced. This may account for the abundant, large, optically continuous patches of quartz observed in the matrix of Sudbury Breccia samples in this study and others (*e.g.*, Morrison *et al.* 1994).

The alteration of biotite to epidote or chlorite (Figs. 5b, c, d, e) resulted in the release of mineral-bound K, allowing the stabilization of K-feldspar:

$$2.5\ K_2(Fe,Mg)_6[Si_6Al_2O_{20}](OH)_4$$
biotite
$$+ 12\ CaAl_2Si_2O_8 + 3\ SiO_2 + 10\ H_2O =$$
anorthite — quartz — fluid

$$1.5\ (Fe,Mg)_{10}Si_6Al_4O_{20}(OH)_{16}$$
chamosite
$$+ 6\ Ca_2Al_3Si_3O_{12}(OH) + 5\ KAlSi_3O_8$$
epidote — K-feldspar

In proximal samples, patches and veinlets of quartz + K-feldspar intergrowth (Fig. 5e) are abundant, and make up to 50 vol.% of the sample. Commonly, these intergrowths have a vuggy core filled with coarse-grained actinolite + epidote + chlorite + biotite clots. Disseminated to blebby sulfides (chalcopyrite ± cubanite ± millerite) comprise up to 5 vol.% of the intergrowth and are late-forming with respect to the silicate minerals. Rocks showing the intergrowth of K-feldspar and quartz were recently classified as a separate rock-type (footwall granophyre) by Molnar *et al.* (2001). They observed that the quartz comprising the intergrowth contains hypersaline (up to 60 wt.% NaCl eq.) primary fluid inclusions. This fluid was interpreted as possibly being magmatic in origin, having exsolved from the cooling SIC (Molnar *et al.* 2001).

There are six major differences that make the diagnostic assemblage described unique to the Sudbury Breccia matrix occurring in proximity to mineralization and dissimilar to the contact-metamorphic assemblages observed in distal samples: (i) actinolite, chlorite, and epidote abundances are higher, and these compose a significant portion (30 to 85 vol.%) of the total volume of the matrix, whereas in distal samples, their combined abundance was not observed to exceed 15 vol.%; (ii) contact-metamorphic pyroxene and hornblende are not preserved; (iii) a chlorite-group mineral is very abundant, not only as a pseudomorph of biotite, but it forms a dense intergrowth with actinolite and epidote in the matrix, whereas in distal samples it was observed primarily as a pseudomorph of biotite; (iv) increased abundance of K-feldspar, and locally very high abundances of the mineral intergrown with quartz; (v) increased abundance of titanite, whereas it was observed only in trace amounts in distal samples, and (vi) locally, preservation of biotite within 10 m of mineralization. The diagnostic retrograde assemblage was easily identified in proximal and peripheral samples because the sample locations (Figs. 2b, c) are less than 600 m from the SIC contact and therefore lie within the former zones of pyroxene and hornblende hornfels of the contact-metamorphic aureole. However, identification of the diagnostic assemblage in samples of Sudbury Breccia matrix collected beyond 600 m from the SIC contact is considerably more difficult because the mineralogy of the diagnostic assemblage and the contact-metamorphic albite–epidote hornfels zone are similar. In such a case, hydroxysilicate abundance alone must be used to identify the diagnostic assemblage, rather than the mineral assemblage alone.

Halogen-Bearing Minerals in Sudbury Breccia Matrix

Amphibole-group phases

Amphibole is the most abundant hydroxysilicate in Sudbury Breccia matrix from all three divisions. Two different populations of amphibole were identified. Type-I amphibole occurs only in distal samples from the hornblende hornfels zone of the contact-metamorphic aureole, and is present as dark brown-green clots (all colors described in plane-polarized light), composed of several subhedral to euhedral grains (0.1 to 0.4 mm in maximum dimension) which become progressively replaced by type-II amphibole, chlorite, and epidote (Fig. 5a). The maximum modal abundance observed is 5 vol.%, and its distribution in samples is highly irregular. Its brown-green pleochroism, higher indices of refraction compared to type-II amphibole, and diamond-shaped cross-sections suggest that it is magnesio-hornblende or ferrohornblende.

Type-II amphibole (Fig. 5f) is the dominant generation of amphibole in Sudbury Breccia matrix and is very

fine grained (less than 0.03 mm in maximum dimension). In distal Sudbury Breccia matrix, it occurs as fibrous clots and bundles, and is colorless to pale brown-green-yellow. Type-II amphibole typically forms pseudomorphic replacements of calcic pyroxene and type-I amphibole, as described above. In proximal and peripheral divisions, type-II amphibole occurs as pale to dark green acicular grains and aggregates of grains in complex intergrowths with epidote, plagioclase and quartz, and partially mantled and replaced by chlorite. The change in color with proximity to mineralization reflects compositional changes (see below). A blue-green pleochroism was also observed in type-II amphibole in proximity to mineralization, a characteristic

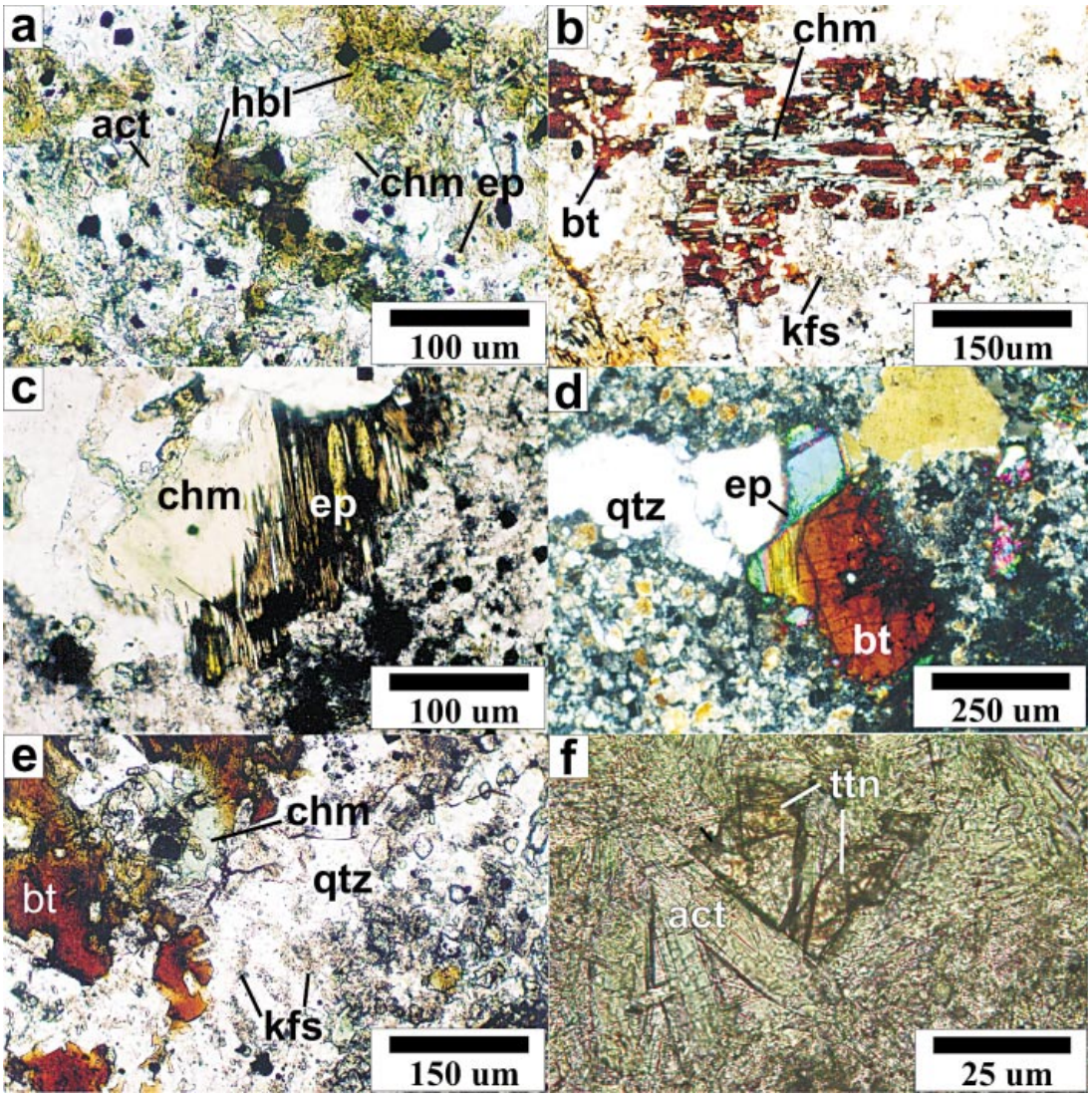

FIG. 5. Photomicrographs of minerals and mineral replacements in Sudbury Breccia matrix. The opaque phases in all images are oxides, mainly titaniferous magnetite. a. Hornblende (hbl) in a transitional sample (hbl hornfels to ab–ep hornfels facies) is mantled by actinolite (act), chamosite (chm), and epidote (ep). Plane-polarized light. b. Biotite (bt) partly replaced by chamosite (chm). K-feldspar (kfs) intergrown with quartz surrounding the biotite. Plane-polarized light. c. Chamosite (chm) pseudomorph after biotite partly replaced by epidote. Plane-polarized light. (d) Biotite (bt) partly replaced by epidote (ep). Crossed nicols. (e) Biotite (bt) partly replaced by chamosite (chm) with K-feldspar (kfs) intergrown with quartz around the alteromorph. Plane-polarized light. (f) Titanite (ttn) interstitial to acicular grains of actinolite (act). Plane-polarized light.

reported in amphiboles from mineralized footwall breccia at the Fraser mine (McCormick & McDonald 1999). In mineralized samples of matrix, type-II amphibole rims, is included in, or is partially replaced by, chalcopyrite and cubanite. The optical properties and electron-microprobe data for type-II amphibole indicate that it is actinolite.

Although type-II amphibole occurs in all three divisions of Sudbury Breccia matrix, it is most abundant in samples from proximal and peripheral divisions. In distal samples, type-II amphibole occurs at modal abundances of less than 15 vol.%, decreasing to trace amounts nearest the SIC, where the mineral assemblage contains pyroxene instead of amphibole. In proximal and peripheral samples, type-II amphibole composes 15 to 60 vol.% of the mode, averaging 35 vol.% in all samples examined. The abundance of type-II amphibole, among other hydroxysilicates (see below), makes proximal and peripheral Sudbury Breccia matrix readily distinguishable from the matrix of distal samples of Sudbury Breccia. Hanley (2002) found that type-II amphibole contributes significantly to the bulk-rock Cl and Br content of the Sudbury Breccia matrix.

Biotite and chlorite

Biotite is a minor constituent of the Sudbury Breccia matrix, occurring in modal abundances of less than 5 vol.% as decussate-textured poikiloblasts (0.25 to 2 mm in diameter) enclosing plagioclase and quartz (Fig. 4a). In distal samples, biotite is locally replaced by chlorite (Fig. 5b). In peripheral and proximal samples, biotite has been replaced almost completely by chlorite and epidote (Fig. 5c). In proximal samples, complete or partial pseudomorphism of biotite by epidote alone was commonly observed (Fig. 5d). Additional products of alteration derived from the biotite are titaniferous magnetite (within the alteromorph) and K-feldspar (around the margins of the alteromorph) (Fig. 5e). Titaniferous magnetite occurs as anhedral inclusions in the chlorite

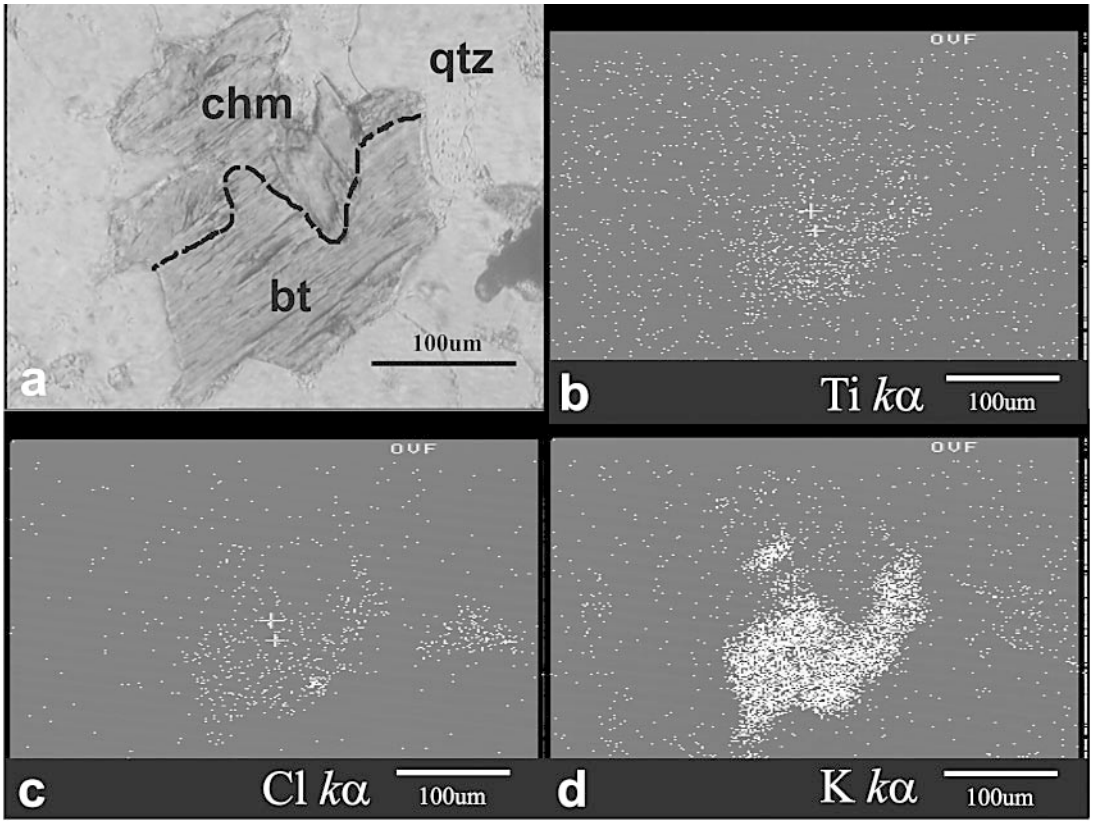

FIG. 6. Photomicrograph and X-ray intensity maps demonstrating the loss of mineral-bound elements from biotite as it alters to chlorite. a. Photomicrograph showing biotite (bt) partly replaced by chamosite (chm), hosted in a quartz (qtz) b. Ti*K*α. c. Cl*K*α. d. K*K*α.

or epidote alteromorph. Images of *K*α X-ray intensity (Hanley 2002) demonstrate that Cl, Ti, and K were rejected by the chlorite during replacement of biotite (Figs. 6a–d).

In close proximity to mineralization, biotite has a brilliant red-brown color. The color changes with increasing distance from mineralization to chestnut-brown in peripheral samples to pale yellow in distal samples. Similarly, the color of chlorite changes from pale yellow to intense green, and that of epidote replacing biotite changes from colorless to yellow with increasing distance from mineralization. These color variations result from changes in Fe content (see below).

In addition to pseudomorphs after biotite, chlorite also occurs as platy to massive, colorless to green clots in the matrix groundmass. High abundances (10 to 40 vol.%) of chlorite (other than replacing biotite) were observed in proximal and peripheral samples. In comparison, the chlorite abundance in the distal samples is much lower (less than 2 vol.%). Like type-II amphibole, the abundance of chlorite makes proximal and peripheral Sudbury Breccia matrix readily distinguishable from distal samples. Hanley (2002) found that chlorite, like amphibole, contributes significantly to the bulk-rock Cl content of the Sudbury Breccia matrix.

Titanite

Titanite (Fig. 5f) occurs in trace amounts as subhedral grains or grain aggregates associated with epidote and type-II amphibole along the margin of hydroxysilicate grains, and in cavities and embayments within chlorite, epidote, or chlorite + epidote pseudomorphs after biotite. Grains are generally much less than 0.05 mm (maximum width) in size and are commonly color-zoned. The abundance of titanite in the Sudbury Breccia matrix appears to be related to epidote abundance and increases with proximity to mineralization, perhaps resulting from alteration by Ca-rich fluids. Such fluids have been observed trapped in alteration minerals directly associated with footwall mineralization (Farrow 1995, Molnar *et al.* 2002, Hanley 2002). Owing to its low modal abundance, titanite contributes negligibly to the bulk-rock Cl content of the Sudbury Breccia matrix.

Apatite

Apatite is rare in Sudbury Breccia matrix and occurs as small, euhedral grains included within biotite poikiloblasts, or in contact with epidote, denoting a possible association between those Ca-rich phases. The grains are typically less than 3 μm across (maximum length), and no more than one or two grains were observed per thin section. Its low abundance and small grain-size (making it difficult to accurately analyze with an electron microprobe) precludes further investigation.

Ferropyrosmalite

The occurrence of this fine-grained phase (less than 50 μm in maximum dimension) is limited to mineralized samples of Sudbury Breccia matrix. The ferropyrosmalite occurs as small, anhedral inclusions in binary chalcopyrite + cubanite grains. The inclusions of ferropyrosmalite do not seem to be spatially related to any fluid inclusion pits or fractures in the sulfide hosts; rather, they occur as solid inclusions in sulfide, which is an indication that the ferropyrosmalite and sulfide crystallized together or that it may have stabilized during the exsolution of Cl from the sulfide fraction during cooling. Ferropyrosmalite occurrences are confined to within 3 m of massive sulfide veins in mineralized areas.

Epidote

Epidote was observed occurring in three associations. Anhedral to subhedral grains (up to 200 μm in maximum dimension) were observed intergrown with actinolite and partially replaced by chlorite in samples from all three classifications. Its modal abundance in this association increases from less than 2 vol.% in distal samples to at least 8 vol.% in peripheral and proximal samples. Epidote was also observed replacing biotite, commonly in association with chlorite, and plagioclase that was formerly poikilitically enclosed in biotite. We did not detect F and Cl in epidote in preliminary electron-microprobe analyses, indicating that epidote does not control bulk-rock halogen abundances.

Analytical Methods

Biotite, amphibole, chlorite, titanite, and ferropyrosmalite were analyzed using wavelength-dispersion spectrometry by means of a Cameca SX–50 electron microprobe at the University of Toronto. The microprobe was operated at 20 kV accelerating voltage, with a beam current of 60 nA to determine halogen concentrations, and 20 nA for all other elements (Si, Ti, Al, Fe, Cr, Mn, Mg, Ca, Na, K). A 10-μm beam was used with on-peak counting times of 30 seconds for the halogens and 10 seconds for other elements. A variety of synthetic and natural oxide, sulfide, and silicate standards were used to calibrate all elements other than the halogens. Fluorine was calibrated using natural fluorite, and Cl was calibrated using natural tugtupite, $NaAlBeSi_4O_{12}Cl$. Preliminary analyses for Br and I showed that these elements are present in abundances below the detection limits attainable in routine analyses.

Analytical accuracy was monitored by analyzing glass of tugtupite composition, basaltic glass, and F-bearing phlogopite standards. The accuracy of results was within 5% for all elements other than F and Cl,

which were within 20 and 4%, respectively. Routine limits of detection (considered to be three standard deviations above background) were 0.05 and 0.008 elemental wt.% for F and Cl, and 0.02 elemental wt.% for all other elements. Neither F nor Cl showed any significant variation in count rate with prolonged and repeated exposure of a spot to the electron beam.

The raw electron-microprobe data were reduced using Probe for Windows© software (J. Donovan, Advanced Microbeam, Inc.), which uses standard ZAF correction algorithms. Mineral formulae were recalculated using the software package MinPet© or using spreadsheet routines. The details of mineral-specific recalculations are described in the following section.

Results of the Analyses

Analyses of hydroxysilicates were made on 23 samples of Sudbury Breccia matrix occurring in the three divisions described and one sample of sulfide-mineralized Sudbury Breccia matrix in contact with a chalcopyrite vein from Zone 38 of the Fraser Copper zone. Results of two or three analyses per grain were averaged to produce the single-grain compositions reported here.

Amphibole

Amphibole compositions appear in Table 1. They were recalculated on the basis of 23 (O,F,Cl) atoms per formula unit (*apfu*), using the method proposed by Robinson *et al.* (1982), in which one calculates the ferric and ferrous ion content by averaging the results obtained assuming a total of 13 cations excluding Ca, Na, and K, and assuming a total of 15 cations excluding Na and K. This method has been shown to reproduce the result of Fe^{3+} determination by wet-chemical analyses of amphiboles to within 28% relative precision (Jobstraibizer & De Pieri 1984). Errors in Fe content are propagated through the recalculated formula of the amphibole. Typical relative precisions of 3% on ^{IV}Al and 20% on the *A*-site occupancy were determined in the same study. Figures 7a and 7b show the classification of amphiboles from Sudbury Breccia matrix based on the criteria established by the IMA subcommittee on amphiboles (Leake 1997). The majority (98% of all determinations) of type-II amphiboles analyzed are actinolitic [ideal composition: $Ca_2(Mg,Fe^{2+})_5[Si_8O_{22}](OH,F,Cl)_2$] in composition, trending toward more Si-poor actinolite or, rarely, Si-rich magnesiohornblende in the proximal and peripheral samples. Some type-II

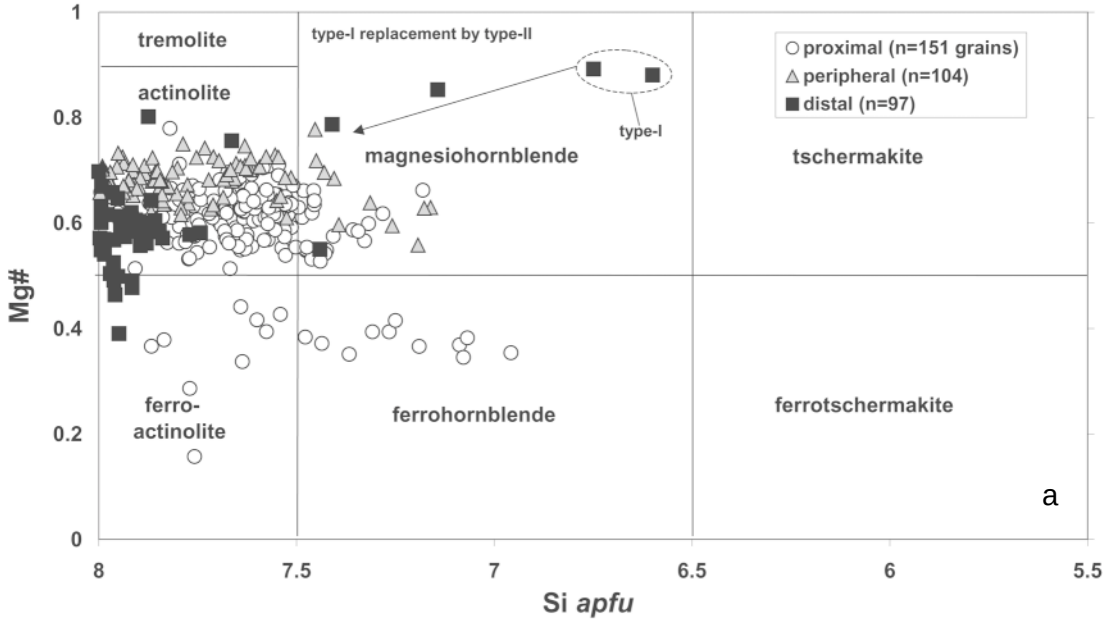

FIG. 7. Classification of amphibole from Sudbury Breccia matrix (after Leake 1997). a. Calcic amphiboles with $^{A}(Na + K) < 0.5$ and Ti (*apfu*) < 0.5 comprise all amphibole analyzed from distal, proximal, and peripheral samples. Type-II amphibole is dominantly actinolite, trending to lower Si content and lower Mg# with proximity to mineralization. These trends correlate with increasing Cl content and Cl/(Cl + F). Type-I amphibole (found only in distal samples) is magnesiohornblende. b. Calcic amphibole with $^{A}(Na + K) < 0.5$ and Ti < 0.5 *apfu* comprise type-II amphibole analyzed from mineralized Sudbury Breccia matrix at the contact between sulfide and Sudbury Breccia host rock. This amphibole is hastingsite.

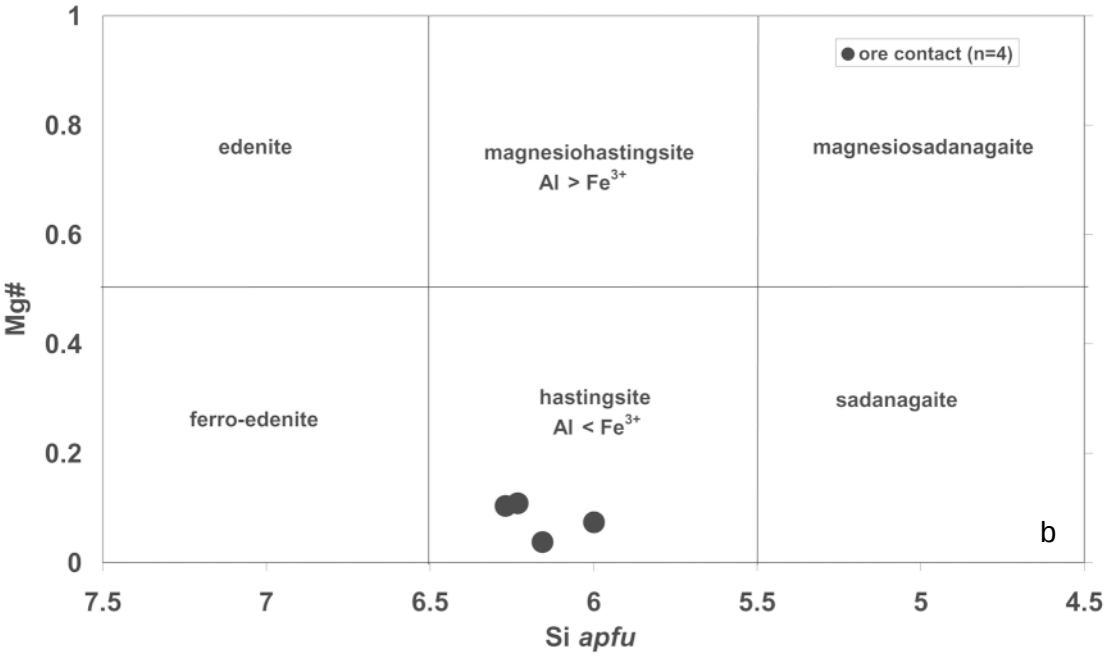

FIG. 7b.

amphiboles (2% of the total determinations) from proximal samples display a weak trend of decreasing Mg# [= $Mg/(Mg + Fe^{2+})$ on an *apfu* basis] with decreasing Si, and tend toward ferroactinolite and ferrohornblende compositions. The type-II amphibole from sulfide-mineralized Sudbury Breccia matrix at the ore contact has a $^{A}(Na + K)$ greater than 0.50 *apfu*, and is classified as hastingsite. For comparison, type-I amphiboles (found only in distal samples from the hornblende hornfels zone) are Si-poor, Mg-rich magnesiohornblende.

The chlorine content of type-II amphibole increases with proximity to mineralization and is strongly related to cation population. The strongest correlation involves K and Cl (Fig. 8). This correlation is typical of amphiboles that have crystallized in a Cl-rich environment (Morrison 1991, Farrow 1995). Similar correlations

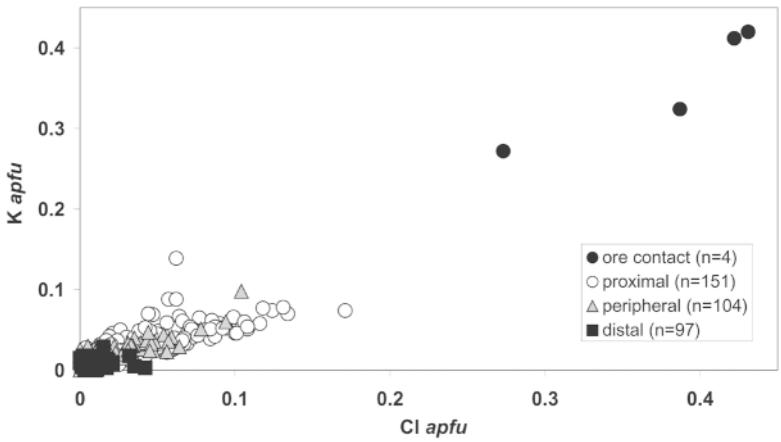

FIG. 8. A plot of K *versus* Cl (*apfu*) (all data) for type-II amphibole, showing a positive correlation. Of all the cations, K demonstrates the strongest correlation with Cl.

TABLE 1. AVERAGE COMPOSITIONS OF AMPHIBOLE FROM SUDBURY BRECCIA MATRIX AND CU-NI-PGE ORE CONTACT (Hanley, 2002)

Sample	Q4	B2M17	B2M5	NEM0	B2M30	SEM45	NEM75	NE-7	SE194	SE71	37-240-8	37-240-6	SB88	JHB315	SB20	SB20	Q4
n grains	2	87	24	14	24	14	3	43	21	23	19	49	20	2	5	2	4
Division	prox	prox	prox	prox	prox	periph	periph	periph	periph	periph	dist	dist	dist	dist	dist	dist	ore
Amphibole	type-II	type-II	type-II	type-II	type-II	type-II	type-II	type-II	type-II	type-II	type-II	type-II	type-II	type-II	type-II	type-I	type-II
SiO_2 wt%	50.93	52.05	51.01	51.97	47.38	52.03	51.49	55.44	52.37	51.24	55.77	52.84	54.94	54.35	53.12	45.81	37.74
TiO_2	0.25	0.37	0.61	0.11	0.08	0.30	0.07	0.07	0.04	0.28	0.04	0.03	0.23	0.05	0.26	0.05	n.d.
Al_2O_3	3.07	2.45	3.93	4.27	4.33	3.57	2.69	1.55	2.51	2.73	1.02	0.90	1.36	1.10	4.11	6.97	11.92
FeO	18.79	16.57	18.73	13.72	25.09	13.61	14.23	13.40	13.16	13.59	13.07	16.58	15.70	13.90	13.22	15.45	30.75
Cr_2O_3	n.d.	0.03	0.03	0.03	n.d.	0.03	n.d.	n.d.	0.03	n.d.	n.d.	n.d.	0.03	n.d.	n.d.	0.06	n.d.
MnO	0.67	0.22	0.33	0.13	0.68	0.17	0.28	0.17	0.18	0.21	0.25	0.24	0.24	0.26	0.21	0.16	0.40
MgO	11.99	13.42	11.38	13.72	6.83	13.89	14.03	15.18	14.56	14.68	14.79	12.41	13.10	14.51	15.67	16.24	1.26
CaO	10.88	11.56	10.08	13.12	11.58	12.35	13.42	12.05	12.52	12.21	11.63	12.49	11.49	12.99	8.65	8.62	11.20
Na_2O	0.53	0.55	0.81	0.31	0.41	0.42	0.30	0.34	0.17	0.47	0.10	0.14	0.13	0.12	0.15	0.22	1.10
K_2O	0.15	0.17	0.30	0.09	0.25	0.13	0.08	0.08	0.06	0.17	0.03	0.04	0.04	0.04	0.10	0.05	1.71
F	0.05	0.12	0.13	0.06	0.05	0.10	0.06	0.12	0.12	0.13	0.09	0.08	0.11	0.10	0.09	0.09	n.d.
Cl	0.15	0.18	0.38	0.06	0.15	0.12	0.03	0.02	0.03	0.16	0.02	0.05	0.02	0.01	0.02	0.04	1.36
Subtotal	97.45	97.65	97.71	97.56	96.82	96.68	96.69	98.43	95.73	95.88	96.81	95.80	97.36	97.42	95.60	93.72	97.45
O=Cl,F	0.06	0.09	0.14	0.04	0.05	0.07	0.03	0.06	0.06	0.09	0.04	0.04	0.05	0.05	0.04	0.05	0.30
Total	97.40	97.56	97.56	97.52	96.77	96.61	96.66	98.37	95.67	95.79	96.77	95.76	97.31	97.37	95.56	93.67	97.15
Cations calculated on the basis of 23 (O,F,Cl) p.f.u. and the average ferric iron constraint (values obtained from the average of 15eNK and 13 eCNK)																	
Si p.f.u.	7.52	7.63	7.56	7.57	7.33	7.64	7.59	7.94	7.72	7.58	8.09	7.94	8.03	7.92	7.62	6.67	6.16
Al^{IV}	0.47	0.36	0.44	0.42	0.66	0.36	0.37	0.08	0.27	0.41	0.00	0.07	0.04	0.08	0.36	1.17	1.84
Fe^{3+}	0.01	0.01	0.00	0.01	0.01	0.00	0.04	0.00	0.01	0.02	0.00	0.00	0.00	0.00	0.03	0.16	0.00
T sites	8.00	8.00	8.00	8.00	8.00	8.00	8.00	8.02	8.00	8.00	8.10	8.00	8.06	8.00	8.02	8.00	8.00
Al^{VI}	0.07	0.06	0.24	0.31	0.13	0.26	0.10	0.18	0.17	0.07	0.17	0.09	0.20	0.11	0.33	0.03	0.46
Cr	0.00	0.00	0.00	0.00	0.00	0.00	0.00	0.00	0.00	0.00	0.00	0.00	0.00	0.00	0.00	0.01	0.00
Fe^{3+}	0.47	0.27	0.42	0.14	0.44	0.15	0.23	0.08	0.14	0.23	0.06	0.01	0.08	0.00	0.59	1.27	0.71
Ti	0.03	0.04	0.07	0.01	0.01	0.03	0.01	0.01	0.00	0.03	0.00	0.00	0.03	0.01	0.03	0.01	0.00
Mg	2.64	2.93	2.51	2.97	1.57	3.04	3.08	3.24	3.20	3.23	3.20	2.78	2.85	3.15	3.35	3.53	0.31
Fe^{2+}	1.76	1.68	1.73	1.49	2.79	1.47	1.48	1.48	1.44	1.41	1.51	2.08	1.82	1.69	0.67	0.15	3.48
Mn	0.04	0.01	0.02	0.01	0.06	0.01	0.02	0.01	0.01	0.01	0.02	0.03	0.02	0.03	0.01	0.01	0.04
Ca	0.00	0.00	0.00	0.05	0.00	0.01	0.08	0.01	0.03	0.01	0.03	0.01	0.01	0.01	0.00	0.00	0.00
C sites	5.00	5.00	5.00	5.00	5.00	5.00	5.00	5.00	5.00	5.00	5.00	5.00	5.00	5.00	5.00	5.00	5.00
Mg	0.00	0.00	0.00	0.00	0.00	0.00	0.00	0.00	0.00	0.00	0.00	0.00	0.00	0.00	0.00	0.00	0.00
Fe^{2+}	0.09	0.07	0.17	0.03	0.01	0.05	0.01	0.05	0.03	0.03	0.02	0.00	0.03	0.00	0.29	0.30	0.00
Mn	0.04	0.01	0.02	0.01	0.03	0.01	0.01	0.01	0.01	0.01	0.01	0.00	0.01	0.00	0.01	0.01	0.02
Ca	1.72	1.82	1.60	1.93	1.92	1.88	1.95	1.84	1.92	1.91	1.78	1.99	1.79	2.00	1.33	1.35	1.96
Na	0.08	0.07	0.11	0.01	0.02	0.04	0.02	0.06	0.02	0.04	0.03	0.00	0.03	0.00	0.03	0.03	0.02
B sites	1.93	1.97	1.90	1.97	1.98	1.98	1.99	1.96	1.98	2.00	1.83	2.00	1.86	2.00	1.66	1.69	2.00
Ca	0.00	0.00	0.00	0.06	0.00	0.02	0.10	0.00	0.03	0.01	0.00	0.01	0.00	0.02	0.00	0.00	0.00
Na	0.08	0.09	0.12	0.08	0.10	0.07	0.07	0.04	0.03	0.09	0.00	0.04	0.00	0.03	0.01	0.03	0.33
K	0.03	0.03	0.06	0.02	0.05	0.02	0.02	0.01	0.01	0.03	0.01	0.01	0.01	0.01	0.02	0.01	0.36
A sites	0.11	0.12	0.17	0.16	0.15	0.14	0.18	0.05	0.07	0.14	0.01	0.05	0.01	0.06	0.03	0.04	0.69
cations	15.03	15.09	15.08	15.13	15.13	15.11	15.17	15.03	15.05	15.13	14.93	15.05	14.94	15.06	14.71	14.73	15.69
Cl	0.04	0.12	0.10	0.01	0.04	0.03	0.01	0.01	0.01	0.04	0.00	0.01	0.00	0.00	0.01	0.01	0.38
F	0.02	0.44	0.06	0.03	0.02	0.04	0.03	0.05	0.06	0.06	0.04	0.04	0.05	0.05	0.04	0.04	0.00
oxygen	23.00	23.02	23.12	23.10	23.00	23.10	23.09	23.09	23.04	23.02	23.13	23.06	23.13	23.05	23.00	22.69	23.00
Cl/(Cl + F)	0.64	0.63	0.61	0.37	0.56	0.31	0.31	0.09	0.11	0.39	0.10	0.24	0.10	0.05	0.10	0.24	0.99
Fe^{3+}/Fe^{2+}	0.25	0.59	0.23	0.23	0.16	0.11	0.15	0.05	0.19	0.17	0.05	0.00	0.04	0.00	0.76	2.82	0.21
Mg#	0.59	0.12	0.57	0.66	0.36	0.67	0.67	0.68	0.68	0.69	0.68	0.57	0.61	0.65	0.78	0.89	0.08
X_{Mg}	0.53	0.44	0.50	0.59	0.31	0.61	0.62	0.65	0.64	0.65	0.64	0.56	0.57	0.63	0.67	0.71	0.06

Samples: prox: proximal; periph: peripheral; dist: distal; ore: contact between mineralized proximal Sudbury Breccia matrix and footwall sulphides.
n.d. - none detected; p.f.u. - atoms per formula unit

exist between Na and Cl, and *A*-site occupancy and Cl. Silicon and Cl (Fig. 9) demonstrate a weakly negative correlation. Increasing Cl/(Cl + F) (*apfu* basis) does not correlate well with decreasing Mg# (Fig. 10). The Mg–Cl and Fe–F avoidance (Ramberg 1952, Rosenberg & Foit 1977) thus do not seem to be major controls on halogen abundance, or other compositional variables have masked this correlation (*i.e.*, the halogen content of the equilibrating fluid).

Biotite

Representative compositions of biotite from the matrix of Sudbury Breccia are presented in Table 2. Structural formulae were recalculated on the basis of 24 (O,OH,F,Cl) *apfu*. Figure 11 shows a classification of the biotite compositions based on their content of ^{IV}Al (*apfu*) and Fe# (= $Fe^{2+}/[Fe^{2+} + Mg]$, atom proportion). The transition from distal samples through peripheral

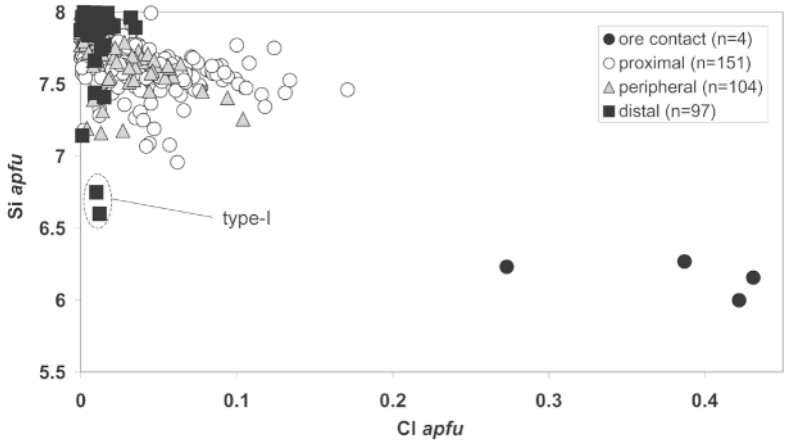

FIG. 9. A plot of Si *versus* Cl (*apfu*) (all data) for type-II amphibole, showing a weak negative correlation.

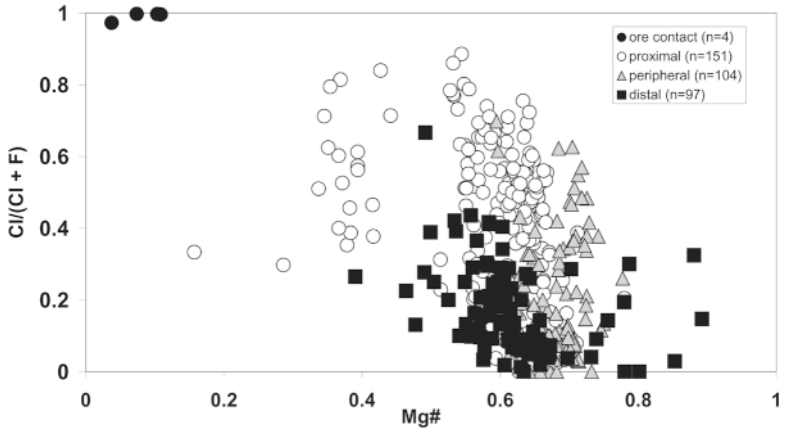

FIG. 10. A plot of Cl/(Cl + F) *versus* Mg# for type-II amphibole, demonstrating a lack of correlation, consistent with Mg–Cl and Fe–F avoidance principles being non-significant controls on halogen content in type-II amphiboles other than for those found along sulfide – host-rock contacts.

TABLE 2. AVERAGE COMPOSITIONS OF BIOTITE FROM SUDBURY BRECCIA MATRIX AND CU-NI-PGE ORE CONTACTS (Hanley, 2002)

Sample	JHC-1	Q4	B2M0	BM20	2C1	2C3	SEM30	NE7-1	NEM20	NEM75	SB20	SB88	Q4
n grains	17	8	17	6	5	7	19	31	23	34	7	6	10
Division	prox	prox	prox	prox	periph	periph	periph	periph	periph	periph	dist	dist	ore
SiO_2 wt%	37.80	36.16	36.31	37.62	38.34	38.54	34.94	37.99	37.61	38.06	36.62	37.60	33.64
TiO_2	3.97	3.79	3.59	3.86	3.39	3.97	3.63	2.41	2.92	3.88	3.54	3.32	1.33
Al_2O_3	12.14	13.54	13.13	13.03	12.68	12.17	12.38	13.82	13.63	13.01	12.80	12.51	12.52
Cr_2O_3	n.d.	0.06	0.05	0.05	n.d.	0.04	n.d.	n.d.	n.d.	0.06	n.d.	0.04	n.d.
FeO	17.89	24.69	20.47	20.48	18.24	16.39	20.16	21.00	21.77	18.94	16.19	16.46	33.42
MnO	0.17	0.22	0.19	0.15	0.18	0.16	0.19	0.19	0.21	0.17	0.16	0.13	0.30
MgO	13.42	7.79	9.69	11.03	12.31	14.25	10.87	10.99	10.35	12.10	14.45	13.90	3.63
CaO	0.18	0.03	0.12	0.04	0.19	0.18	0.17	0.11	0.08	0.06	0.06	0.19	0.05
Na_2O	0.08	0.05	0.09	0.04	0.23	0.10	0.11	0.09	0.07	0.10	0.06	0.07	0.06
K_2O	8.68	9.11	8.61	9.13	8.97	8.92	9.02	9.11	9.16	9.31	8.13	7.68	8.28
F	0.25	0.10	0.31	0.37	0.23	0.21	0.12	0.15	0.14	0.16	0.48	0.49	0.08
Cl	0.25	0.17	0.24	0.17	0.17	0.17	0.10	0.10	0.09	0.09	0.15	0.16	1.77
H_2O	5.14	4.30	7.22	4.03	5.05	4.89	8.30	4.00	3.97	4.05	7.35	7.45	4.92
Subtotal	100.00	100.00	100.00	100.00	100.00	100.00	100.00	100.00	100.00	100.00	100.00	100.00	100.00
O=Cl,F	0.16	0.08	0.18	0.19	0.14	0.13	0.07	0.09	0.08	0.09	0.24	0.25	0.43
Total	99.84	99.92	99.82	99.81	99.86	99.87	99.93	99.91	99.92	99.91	99.76	99.76	99.57
Cations calculated on the basis of 24 (O,OH,F,Cl)													
Si p.f.u.	5.63	5.61	5.36	5.74	5.72	5.71	5.11	5.79	5.76	5.76	5.29	5.40	5.50
Al^{IV}	2.13	2.38	2.27	2.25	2.22	2.12	2.13	2.21	2.24	2.19	2.17	2.12	2.37
Al^{VI}	0.00	0.09	0.00	0.10	0.00	0.00	0.00	0.27	0.22	0.13	0.00	0.00	0.04
Ti	0.45	0.44	0.40	0.44	0.38	0.44	0.40	0.28	0.34	0.44	0.39	0.36	0.16
Fe^{2+}	2.23	3.20	2.52	2.62	2.28	2.03	2.46	2.68	2.79	2.40	1.95	1.98	4.58
Cr	0.00	0.01	0.01	0.01	0.00	0.01	0.00	0.00	0.00	0.01	0.00	0.00	0.00
Mn	0.02	0.03	0.02	0.02	0.02	0.02	0.02	0.02	0.03	0.02	0.02	0.02	0.04
Mg	2.98	1.80	2.13	2.51	2.74	3.15	2.37	2.49	2.36	2.73	3.11	2.98	0.88
Ca	0.03	0.00	0.02	0.01	0.03	0.03	0.03	0.02	0.01	0.01	0.01	0.03	0.01
Na	0.02	0.01	0.02	0.01	0.07	0.03	0.03	0.03	0.02	0.03	0.02	0.02	0.02
K	1.65	1.80	1.62	1.78	1.71	1.69	1.68	1.77	1.79	1.80	1.50	1.41	1.73
cations	15.14	15.39	14.38	15.48	15.16	15.22	14.23	15.56	15.55	15.51	14.46	14.32	15.32
F	0.24	0.10	0.29	0.35	0.22	0.19	0.11	0.15	0.13	0.16	0.44	0.45	0.08
Cl	0.13	0.09	0.12	0.09	0.09	0.09	0.05	0.05	0.05	0.05	0.08	0.08	0.99
OH	5.10	4.44	7.08	4.10	5.02	4.83	8.10	4.07	4.05	4.08	7.06	7.14	5.36
Cl/F	0.55	0.89	0.41	0.25	0.39	0.44	0.45	0.35	0.34	0.30	0.17	0.17	12.56
Cl/(Cl + F)	0.34	0.47	0.29	0.20	0.29	0.31	0.31	0.27	0.26	0.24	0.15	0.15	0.88
X_{Cl}	0.02	0.02	0.02	0.02	0.02	0.02	0.01	0.01	0.01	0.01	0.01	0.01	0.15
X_F	0.04	0.02	0.04	0.08	0.04	0.04	0.01	0.03	0.03	0.04	0.06	0.06	0.01
Mg#	0.57	0.36	0.46	0.49	0.55	0.61	0.49	0.48	0.46	0.53	0.61	0.60	0.16
X_{Mg}	0.57	0.36	0.45	0.49	0.54	0.60	0.49	0.48	0.46	0.53	0.61	0.60	0.16
X_{sid}	0.11	0.27	0.20	0.16	0.12	0.07	0.18	0.20	0.21	0.14	0.13	0.09	0.34
X_{ann}	0.33	0.37	0.35	0.36	0.34	0.32	0.34	0.32	0.34	0.33	0.26	0.31	0.50
$I_{(F\text{-}Cl)}$	6.87	6.40	6.38	6.27	6.64	6.89	6.52	6.38	6.30	6.47	6.49	6.45	6.94
$\log(f_{HCl}/f_{HF})$	2.92	2.45	2.43	2.33	2.69	2.94	2.57	2.43	2.35	2.52	2.54	2.51	2.99

Samples: prox: proximal; periph: peripheral; dist: distal; ore: contact between mineralized proximal Sudbury Breccia matrix and footwall sulphides. n.d.: not detected; p.f.u.: atoms per formula unit; X_{sid}: siderophyllite component; X_{ann}: annite component; $I_{(F\text{-}Cl)}$: F-Cl intercept value (Munoz, 1984) Total Fe reported as FeO. H_2O calculated by difference. Recrystallization temperature taken from amphibole-plagioclase thermometry (Table 4) and used to calculate $\log(f_{HCl}/f_{HF})$ using eq'n *1* (see text) is 500°C

and proximal samples through to the ore contacts correlates with increasing annite (X_{ann}) and siderophyllite (X_{sid}) content in the biotite. Biotite from distal samples have compositions nearest the annite–phlogopite join [ideal composition: $K_2(Fe,Mg)_6(Si_6Al_2O_{20})(OH,F,Cl)_4$], whereas biotite from the ore contacts has a composition nearest the siderophyllite–annite join [ideal composition: $K_2(Mg)_{4–6}(Al)_{0–2}(Si_{4–6}Al_{2–4}O_{20})(OH,F,Cl)_4$].

In contrast to type-II amphiboles, Mg–Cl or Fe–F avoidance is well developed in biotite from Sudbury Breccia matrix. Figure 12 shows Cl/(Cl + F) *versus* Mg# for biotite from Sudbury Breccia matrix plotted along with compositions from Ni–Cu–PGE deposits in a plot modified from Farrow & Watkinson (1999). High-Cl, low-Mg annite from sulfide ores of three footwall vein-type deposits (Fraser Cu zone, Thayer Lindsley, and McCreedy West deposits) define a field labeled "hydrothermal compositions", and low-Cl phlogopite from rocks hosting primary magmatic Ni–Cu–PGE deposits define a field labeled "magmatic compositions". There is a broad compositional trend from the magmatic to the hydrothermal fields, corresponding to the transition from distal to proximal sample settings. No other correlations were made between cations in biotite and the halogen content of biotite in Sudbury Breccia matrix.

Titanite

Representative compositions of titanite [ideal composition: $CaTi(SiO_4)(O,OH,F,Cl)$] in all three sample divisions are listed in Table 3. Contents of Cl and F range from below detection limits to 0.11 wt.% and from 0.06 to 0.26 wt.%, respectively. No variation in halogen content with ore proximity was identified. This result, coupled with low modal abundance, excludes titanite as a major influence on the bulk-rock distribution of Cl and F.

Ferropyrosmalite

Only semiquantitative data were collected for ferropyrosmalite [ideal composition: $(Fe^{2+},Mn)_8Si_6O_{15}(OH,Cl)_{10}$]. Data collection was severely limited by the destructive effects of the electron beam on the mineral, and the very small grain-size (1 to 5 μm in maximum dimension). Ferropyrosmalite occurs within disseminated sulfide in proximal samples and contains greater than 5 wt.% Cl. Ferropyrosmalite could therefore account for a substantial portion of the bulk-rock chlorine encountered in the matrix of proximal Sudbury Breccia, despite its occurrence as only a trace mineral. Semiquantitative analyses for Br content indicate a range from 300 to 500 ppm.

Chlorite

Representative compositions of chlorite are given in Table 3. Based on the classification scheme for chlorite (Deer *et al.* 1972), the chlorite analyzed is chamosite [ideal composition: $(Fe,Mg)_5Si_3Al_2O_{10}(OH)_8$]. Contents of Cl and F are low and range from 310 to 480 ppm, and from 120 to 900 ppm, respectively. The Cl content does not increase with proximity to ore, but owing to the high abundance of chlorite in Sudbury Breccia matrix near

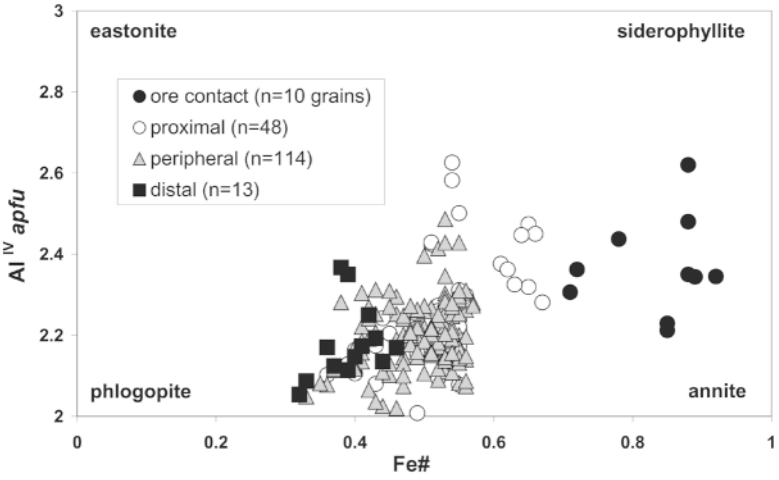

FIG. 11. Classification of biotite (all data) from Sudbury Breccia matrix (after Bailey 1984) based on Fe# and ^{IV}Al content (on an *apfu* basis). Compositions span a range from the midpoint of the phlogopite–annite join trending toward the midpoint of the siderophyllite–annite join with increasing proximity to mineralization.

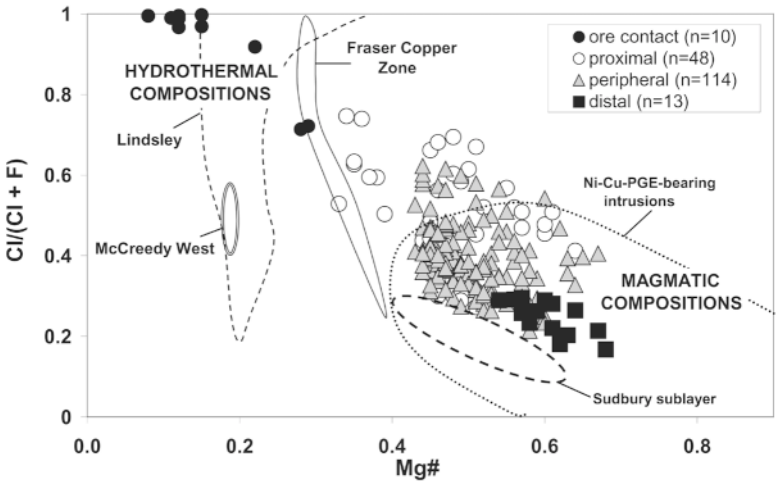

FIG. 12. Plot of Cl/(Cl + F) *versus* Mg# for biotite from Sudbury Breccia matrix (modified from Farrow & Watkinson 1999). Fields for relevant Ni–Cu–PGE environments are plotted. A general trend from magmatic to hydrothermal compositions is exhibited by the biotite as areas of mineralization are approached, demonstrating the control of Mg–Cl and Fe–F avoidance on the halogen content of the biotite. The avoidance principle is best developed in the distal samples, and is more diffuse for biotite from the other divisions, suggesting that an additional factor [temperature, fluid log *f*(HCl)/*f*(HF)], influenced the halogen content of the biotite near areas of mineralization.

TABLE 3. REPRESENTATIVE COMPOSITIONS OF CHLORITE AND TITANITE FROM THE MATRIX OF SUDBURY BRECCIA SAMPLES

	Chlorite				Titanite							
Sample	SB 20	SB 20	Q 4	SEM 30	B2 M17	B2 M25	37-240-8	37-240-6	SB 20	SB 20	SE 71	NE-7
Location	dist	dist	prox	prox	prox	prox	dist	dist	dist	dist	periph	periph
SiO_2 wt%	26.58	26.86	26.37	26.79	30.43	30.27	32.35	30.94	35.57	30.70	30.80	30.74
TiO_2	0.14	n.d.	0.14	0.14	36.91	37.95	36.05	37.11	33.58	35.74	36.90	34.02
Al_2O_3	18.53	18.09	18.35	18.44	1.10	0.55	0.84	1.24	0.71	1.64	1.16	1.82
FeO	25.33	25.33	25.70	25.78	1.53	0.81	1.43	0.63	1.68	1.11	0.93	1.08
MnO	0.17	0.13	0.19	0.20	0.03	0.07	0.06	n.d.	n.d.	n.d.	0.03	n.d.
MgO	14.75	14.84	14.36	14.93	0.03	n.d.	0.05	n.d.	n.d.	n.d.	n.d.	n.d.
CaO	0.07	0.11	0.08	n.d.	28.30	28.49	27.46	27.85	26.40	29.18	29.08	29.01
Na_2O	0.07	0.02	0.11	0.06	0.07	0.07	0.12	0.38	0.40	n.d.	0.09	0.03
K_2O	n.d.	0.08	n.d.	0.04	n.d.	n.d.	n.d.	0.03	0.05	n.d.	n.d.	n.d.
F	n.d.	0.09	n.d.	0.07	0.07	0.08	0.10	0.11	0.06	0.25	0.19	0.26
Cl	0.05	0.03	0.03	0.05	0.03	0.06	0.07	0.10	0.11	n.d.	0.05	0.03
Total	85.69	85.58	85.33	86.51	98.48	98.35	98.52	98.40	98.55	98.61	99.22	97.00

Samples: prox: proximal; periph: peripheral; dist: distal. n.d.: none detected. Total Fe reported as FeO. Low totals may be accounted for by the presence of H2O (not determined).

areas of mineralization, its Cl content contributes significantly to the bulk-rock inventory of Cl.

Discussion

Constraints on alteration temperature and paragenesis

Experimental studies have shown that the upper and lower stability-limits of amphibole in a protolith of intermediate composition similar to that of the Sudbury Breccia matrix are 720 to 770°C, above which hornblende dehydrates to pyroxene, and 300°C, below which actinolite is unstable (*e.g.*, Liou *et al.* 1974, Spear 1981). These constraints are applicable to systems at lithostatic or hydrostatic pressures between 0.5 and 1 kbar, where $X(H_2O)$ of the equilibrating fluid is near 1.

Within each division, estimates of final temperatures of equilibration for type-I amphibole (sample SB20) and type-II amphibole (samples SEM45 and B2M0) in textural equilibrium with plagioclase were determined using the amphibole–plagioclase geothermometer proposed by Blundy & Holland (1990). This mineral thermometer yields temperatures of equilibration ±75°C (absolute 3σ uncertainty) for rocks equilibrated at temperatures in the range of 500 to 1000°C, for assemblages with plagioclase less calcic than An_{92}, and with amphiboles containing less than 7.8 Si *apfu*.

Amphibole–plagioclase compositions and calculated temperatures of equilibration or formation are presented in Table 4. The pressure of formation used in the calculations was 1.3 kbar (5 km), a constraint determined recently from fluid-inclusion studies (Molnar *et al.* 2001), and broadly consistent with the probable position of the sample locations under the SIC at the time of alteration. Two samples of type-I amphibole (hornblende) from distal sample SB20 yielded an estimated temperature of equilibration of 618° and 688°C ± 75°C (*cf.* Molnar *et al.* 2001). Nine measurements on type-II amphibole in proximal sample B2M0 and peripheral sample SEM45 gave a range from 442° to 540°C ± 75°C, consistent with the estimate of Winkler (1967) for the transition from hornblende hornfels to albite–epidote hornfels in the Sudbury footwall. The geothermometer is poorly calibrated below 500°C, but six out of nine determinations of temperature from samples proximal to mineralization gave equilibration temperatures below 500°C. Therefore, in samples near the mineralized areas, we estimate the lower limit of type-II amphibole formation to be significantly below 500°C (see below), and the upper limit of formation to be 615°C.

The generally lower temperatures recorded by the proximal and peripheral mineral assemblages containing type-II amphibole indicate that the diagnostic assemblage is retrograde, having formed at temperatures well below the peak conditions of contact metamorphism. Other indicators for this retrograde process are the disappearance of pyroxene (from rocks formerly in the pyroxene hornfels facies), the appearance of epidote followed by chlorite, and the albitization of plagioclase. The recorded temperatures are independent of distance from the SIC, and reflect only distance from mineralized areas.

The apparent retrograde nature of the diagnostic assemblage can be confirmed for rocks that were previ-

TABLE 4. DATA ON AMPHIBOLE–PLAGIOCLASE PAIRS AND THERMOMETRIC CALCULATIONS, SUDBURY BRECCIA SAMPLES

Sample	SEM 45	SEM 45	SEM 45	SEM 45	SEM 45	SEM 45	SB 20	SB 20	B2 MO	B2 MO	B2 MO	B2 MO	B2 MO
Grain	amp-pl1	amp-pl2	amp-pl3	amp-pl4	amp-pl5	amp-pl6	amp-pl7	amp-pl8	amp-pl9	amp-pl10	amp-pl11	amp-pl12	amp-pl13
Location	periph	periph	periph	periph	periph	periph	dist	dist	prox	prox	prox	prox	prox
Amphibole	type II	type II	type II	type II	type II	type II	type I	type I	type II	type II	type II	type II	type II
Si(amp)	7.79	7.72	7.80	7.73	7.79	7.53	7.41	7.14	7.85	7.75	7.75	7.75	7.77
Ab(pl)	90.90	91.90	96.60	95.40	96.30	95.40	65.60	64.20	56.10	62.70	88.70	65.80	68.40
K	16.57	11.98	18.65	13.28	17.56	7.08	3.79	2.35	14.11	9.49	13.42	9.75	11.26
ln K	2.81	2.48	2.93	2.59	2.87	1.96	1.33	0.86	2.65	2.25	2.60	2.28	2.42
P(kbar)	1.30	1.30	1.30	1.30	1.30	1.30	1.30	1.30	1.30	1.30	1.30	1.30	1.30
T* (K)	726	757	716	747	721	813	891	962	741	781	746	778	763
T* (°C)	453	484	442	474	448	540	618	688	468	508	473	505	490

Samples: prox: proximal; periph: peripheral; dist: distal; ore: contact between mineralized proximal Sudbury Breccia matrix and footwall sulfides. n.d.: none detected. Si(amp): Si atoms per formula unit in amphibole, Ab(pl): albite component of plagioclase, in mol.%. P (kbar) is taken from Molnar *et al.* (2001); T* is the recorded temperature of equilibration or formation of amphibole and plagioclase. K is calculated using Si content of amphibole and Ab component of the plagioclase (formula taken from Munoz 1984).

ously of pyroxene hornfels grade using equilibrium activity diagrams (Figs. 13a–c). Activity diagrams were selected from Bowers *et al.* (1984) for the system HCl–H_2O–(Al_2O_3)–CaO–MgO–SiO_2 at P(H_2O) = 1 kbar and T = 600, 400, and 300°C. In these diagrams, assemblages are assumed to be in equilibrium with quartz (which is present in all samples examined), and the saturation limits for clinopyroxene and tremolitic amphibole are shown as dashed lines. It is apparent from these diagrams that the diagnostic assemblage can only be produced from the original contact-metamorphic assemblage by a progressive decrease in temperature of formation. At 600°C (Fig. 13a), clinopyroxene + anorthite + quartz ± tremolite coexist (compositional field 1), and epidote is absent. Epidote appears between 500 and 400°C, and a small field of stability for epidote in equilibrium with tremolite ± anorthite ± clinopyroxene occurs at T = 400°C (Fig. 13b, compositional field 2). At this temperature, epidote and chlorite may coexist, but this requires clinopyroxene to be present. In all samples examined from the proximal and peripheral divisions, clinopyroxene is absent. Therefore, we infer that the appearance of chlorite was restricted to temperature less than 400°C. This is confirmed in Figure 13c (300°C), where the major components of the diagnostic assemblage, epidote + actinolite–tremolite + chlorite, will coexist only in the absence of clinopyroxene (compositional field 3). Therefore, the appearance of epidote (between 400° and 500°C), followed by the appearance of chlorite with epidote (between 300° and 400°C) confirm the retrograde nature of the diagnostic assemblage. Note that at 300°C, anorthite is absent. Overall, the formation of the diagnostic assemblage requires an increase in the activity of Ca^{2+} and Mg^{2+} of the equilibrating fluid.

The diagnostic assemblage in the proximal and peripheral breccia is classified as belonging to the albite–epidote hornfels facies (Dressler 1984, Fry 1984, Yardley 1989). Changes in mineral assemblage as this retrograde metamorphism progressed are similar to those that occur during the amphibolite-to-greenschist transition (Liou *et al.* 1974, Spear 1981, Moody *et al.* 1983). A modern analogue to these alteration processes in the footwall Cu–Ni–PGE ore systems may be the active greenschist-facies metamorphism of the Salton Sea geothermal system in southern California, which is also known for its high-chloride, high-salinity brines (greater than 25 wt.% dissolved solids) that contain high levels of dissolved base and precious metals, abundant sulfide mineralization at depth, and actively forming greenschist-grade Cl-bearing Fe–Mg–Ca-silicate alteration assemblages (*e.g.*, Skinner *et al.* 1967). This analogue has been recently proposed for other alteration assemblages occurring in footwall-type Cu–Ni–PGE (Farrow 1995) and contact-type Ni–Cu–PGE ores (McCormick & McDonald 1999).

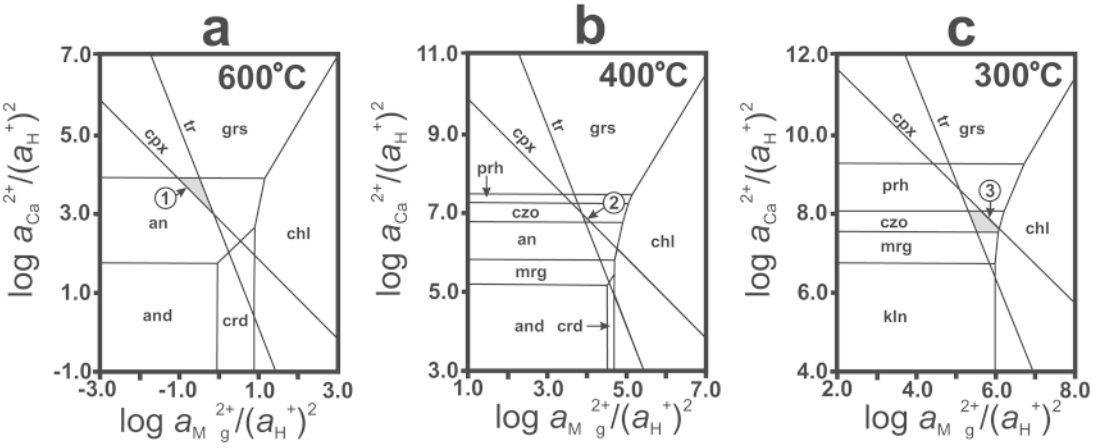

FIG. 13. Activity diagrams selected from Bowers *et al.* (1984) for the system HCl–H_2O–(Al_2O_3)–CaO–MgO–SiO_2 at P(H_2O) = 1 kbar, which demonstrate the retrograde nature of the diagnostic hydrous assemblage. Mineral abbreviations: cpx pyroxene, tr actinolite–tremolite, an anorthite, grs grossular, chl chlorite, and andalusite, crd cordierite, czo clinozoisite (epidote), prh prehnite, mrg margarite, kln kaolinite. a. At 600°C, clinopyroxene + anorthite + quartz ± tremolite coexist (labeled field "1"), and epidote is absent. b. At 400°C, epidote can exist in equilibrium with tremolite ± anorthite ± clinopyroxene (labeled field "2"). At this temperature, epidote and chlorite may coexist, but this requires clinopyroxene to be present. c. At 300°C, the major components of the diagnostic assemblage (epidote + actinolite–tremolite + chlorite) may coexist in the absence of clinopyroxene (labeled field "3"). No pyroxene was observed in any proximal or peripheral samples containing the diagnostic assemblage.

Constraints on fluid halogen content and origin of the fluid

The log [*f*(HCl)/*f*(HF)] of the fluid that last equilibrated with biotite in the matrix of the Sudbury Breccia was determined using the F–Cl intercept method (Munoz 1984). We here denote the F–Cl intercept value as $I_{F–Cl}$. It is a measure of the F/Cl value in biotite, corrected for the effects of Fe–F and Mg–Cl avoidance. It may also be used to derive the log [*f*(HCl)/*f*(HF)] of the fluid that last equilibrated with the mica at a specific temperature of formation as follows:

$$\log [\, f(\mathrm{HCl})/f(\mathrm{HF})] = -3051/T + I_{F–Cl} \quad (1)$$

where $I_{F–Cl}$ is calculated using the components X_{Cl}, X_F, X_{Mg}, X_{sid} and X_{ann} from the biotite (Munoz 1984).

We have shown above that the halogen content of biotite in Sudbury Breccia Matrix correlates only with Mg#. Therefore, by removing any effects of the Fe–F and Mg–Cl avoidance, variation in Cl content entirely due to changes in the halogen content of fluid or temperature of formation may be determined. Calculated values for X_{Cl}, X_F, X_{Mg}, X_{sid}, X_{ann}, $I_{F–Cl}$, and log [*f*(HCl)/*f*(HF)] are summarized in Table 2 for biotite in samples from all three divisions. Figure 14 illustrates the relationship of bulk F/Cl value to the log [*f*(HCl)/*f*(HF)] of the fluid that last equilibrated with the biotite; we assume an equilibration temperature of 500°C, based on the results obtained from amphibole–plagioclase geothermometry, and observe that biotite is preserved in the diagnostic assemblage.

Two significant compositional characteristics of the biotite are evident. First, the bulk F/Cl value of biotite from proximal and peripheral samples is negatively correlated with log [*f*(HCl)/*f*(HF)], defining a trend toward compositions of biotite from the ore contacts. Therefore, independent of avoidance effects, the F/Cl value of biotite from peripheral and proximal samples was determined by the *f*(HCl)/*f*(HF) in the fluid with which it last equilibrated. In comparison, the halogen content of biotite from distal samples is independent of *f*(HCl)/*f*(HF) content in the equilibrating fluid, and such biotite has a higher F/Cl content. These characteristics suggest that biotite in the distal samples has experienced no enrichment in Cl due to secondary hydrothermal processes after its initial formation in the contact-metamorphic assemblage. Its halogen content is strongly dependent on cation- avoidance behavior, as discussed previously. Second, biotite in proximal and peripheral samples has a wider range of intercept values, and therefore a wide range of fluid log [*f*(HCl)/*f*(HF)] values (2.3 to 3.1) compared to those in the distal group (2.4 to 2.7). This observation is very significant because it suggests that

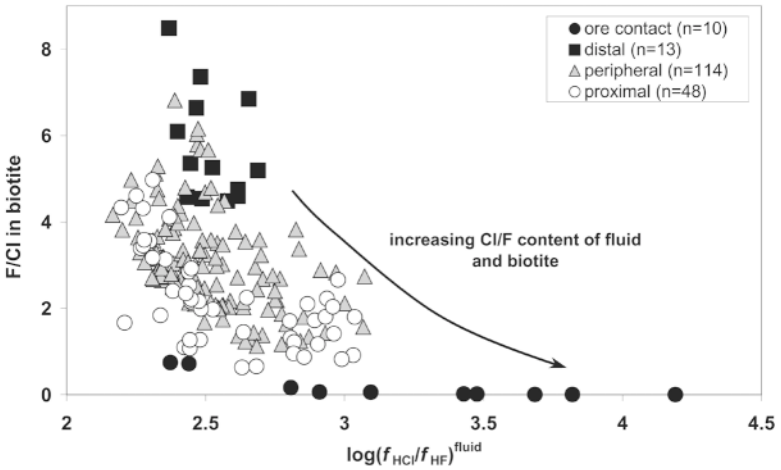

FIG. 14. Plot of the F/Cl ratio in biotite (atom ratio) from Sudbury Breccia matrix *versus* the log [*f*(HCl)/*f*(HF)] for the fluid that last equilibrated with the biotite during matrix recrystallization. The log [*f*(HCl)/*f*(HF)] was calculated using an minimum temperature of re-equilibration of 500°C and the F–Cl intercept value ($I_{F–Cl}$) for the biotite. Independent of cation–halogen avoidance, the halogen content of distal samples of biotite shows no dependence on fluid halogen content, whereas the halogen content of biotite from proximal, peripheral, and contact samples correlates with fluid halogen content. The wide range in log [*f*(HCl)/*f*(HF)] recorded by the biotite from ore-hosting breccias is consistent with recrystallization in the presence of a poorly mixed fluid of variable halogen content.

biotite from the proximal and peripheral groups has been in contact with fluids with more widely varying *f*(HCl)/*f*(HF) during its recrystallization and equilibration, an inference consistent with incomplete mixing of fluids (involving magmatic and metamorphic fluids, or saline groundwaters) or multiple pulses of fluid activity, as suggested by Marshall *et al.* (1999). There are several other indications from this study, notably the correlation in the amphiboles between the *A*-site cations and Cl, and the Ca-rich nature of the diagnostic assemblage, that a genetic link exists between the extremely high salinities (55,600–270,000 ppm Cl^-) and high concentrations of K^+ (37–4700 ppm), Na^+ (7130–34,000 ppm), and Ca^{2+} (19,300–109,000 ppm) in modern and ancient saline and briny groundwaters, and those fluids that gave rise to alteration assemblages associated with footwall-style mineralization (Frape & Fritz 1987, Li 1992, Farrow 1995).

The appearance of the diagnostic assemblage and enrichment in its chlorine content have been demonstrated previously to correlate with bulk-rock Cl, Cl/Br and, Cl/(Cl + F) values (Hanley 2002). In general, the results of this study are consistent with the Cl-enriched alteration halo observed surrounding contact-style Ni–Cu–PGE mineralization at the Fraser mine (McCormick *et al.* 2002). However, on the basis of the observations and arguments presented here, it is unlikely that high bulk-rock Cl contents of proximal and peripheral breccias have resulted from their equilibration with an unusually Cl-rich fluid. Rather, the growth of large volumes of Cl-bearing phases occurred because of the increased stability at lower temperatures of the retrograde Cl-rich diagnostic hydroxysilicate assemblage, which incorporated Cl released during alteration of primary contact-metamorphic minerals (*e.g.*, hornblende, biotite) and, more importantly, Cl contained in large amounts of an aqueous fluid passing through the mineralization-hosting breccias, allowing the hydration reactions described to proceed. This process was aided by the development of cation compositions favorable for incorporation of Cl (K-content in type-II amphiboles, and Mg# in biotite).

Conclusions

We have identified an alteration-induced assemblage of hydrous minerals composed of actinolite + chamosite + epidote + plagioclase + quartz ± titaniferous magnetite ± K-feldspar ± biotite ± titanite, which is unique to the matrix of the Sudbury Breccia within 150 m of footwall Cu–Ni–PGE mineralization at the Fraser mine. The rocks of the pyroxene hornfels and hornblende hornfels facies formerly comprising the contact-metamorphic aureole around the SIC have undergone retrograde alteration to produce the diagnostic hydroxysilicate-rich albite–epidote hornfels assemblage. The defining characteristics of the diagnostic assemblage indicative of proximity to mineralization are: (i) combined modal abundances of actinolite, chlorite, and epidote between 30 and 85 vol.% compared with normal abundances of less than 15 vol.%; (ii) complete replacement of pyroxene and hornblende; (iii) partial to complete replacement of biotite by chlorite or epidote (or both); (iv) increased abundance of K-feldspar, and (v) increased abundance of titanite, which is observed only in trace amounts in distal samples.

Biotite and amphibole in the matrix of the Sudbury Breccia proximal and peripheral to known mineralization are enriched in Cl relative to distal samples. The Cl/(Cl + F) (or Cl/F) values in these phases are higher in the diagnostic assemblage and increase with proximity to mineralization. The *A*-site cations in amphibole are correlated with Cl abundance, consistent with crystallization in equilibrium with Cl-rich fluids. In biotite, Cl-content was regulated by avoidance principles (Mg–Cl and Fe–F), and variations in *f*(HCl)/*f*(HF) in the fluid phase. The temperature of formation of the type-II amphibole in the diagnostic assemblage was between 442° and 540°C ± 75°C, consistent with a suggestion (from petrographic interpretations and theoretical consideration of equilibrium activity diagrams) that the assemblage is retrograde in nature with respect to the contact metamorphic aureole of the SIC. The log [*f*(HCl)/*f*(HF)] value for the fluid that was last in equilibrium with biotite from the diagnostic assemblage is between 2.3 and 3.1, consistent with the hypothesis that mineralizing or post-mineralization fluids were mixtures, or that successive pulses of fluid activity occurred in Sudbury Breccia zones that now host footwall-type mineralization.

The formation of the diagnostic assemblage was the result of secondary hydrothermal activity, postdating formation of the contact-metamorphic aureole of the SIC. During or after emplacement of bodies of footwall-style magmatic Cu–Ni–PGE mineralization, large amounts of Cl-bearing aqueous fluid passed through their hosting Sudbury Breccia zones. Identification of the diagnostic assemblage may help in identifying prospective zones of Sudbury Breccia during the exploration for footwall Cu–Ni–PGE ore systems on the northern margin of the Sudbury Igneous Complex.

Acknowledgements

The authors thank Paul Binney and John Fedorowich of Falconbridge Ltd. (Sudbury Exploration Office) for their guidance and logistical support, and Dave King, Kevin Chisholm, and Al Wilkins of Falconbridge Ltd. (geology of the Fraser and Strathcona mines) for their permission and assistance in accessing underground workings for sampling purposes. J.H. thanks Clayton Capes (Department of Geology, University of Toronto), who assisted greatly with mapping and sampling, and Claudio Cermignani (also at the University of Toronto), who oversaw the development of the electron-microprobe analytical routines. The manuscript was greatly improved by reviews from Catharine Farrow, Enrique

Merino, and Robert F. Martin. Funding for J.M. from Falconbridge Ltd. and NSERC is gratefully acknowledged. Support for J.H. came in the form of an Ontario Graduate Scholarship in Science and Technology and the Ellesworth Scholarship in Mineralogy (Department of Geology, University of Toronto).

References

BAILEY, S.W. (1984): Classification and structures of the micas. In Micas (S.W. Bailey, ed.). *Rev. Mineral.* **13**, 1-12.

BINNEY, W.P., POULIN, R.Y., SWEENY, J.M. & HALLADAY, S.H. (1994): The Lindsley Ni–Cu–PGE deposit and its geological setting. *In* Proc. Sudbury–Noril'sk Symposium (P.C. Lightfoot & A.J. Naldrett, eds.). *Ontario Geol. Surv., Spec. Vol.* **5**, 91-103.

BLUNDY, J.D. & HOLLAND, T.J.B. (1990): Calcic amphibole equilibria and a new amphibole–plagioclase geothermometer. *Contrib. Mineral. Petrol.* **104**, 208-224.

BOUDREAU, A.E., MATHEZ, E.A. & MCCALLUM, I.S. (1986a): Halogen geochemistry of the Stillwater and Bushveld complexes: evidence for transport of the platinum-group elements by Cl-rich fluids. *J. Petrol.* **27**, 967-986.

_____, _____ & _____ (1986b): The role of Cl-rich fluids in the Stillwater Complex, Montana. *Geol. Assoc. Can. – Mineral. Assoc. Can., Program Abstr.* **11**, 47.

BOWERS, T.S., JACKSON, K.J. & HELGESON, H.C. (1984): *Equilibrium Activity Diagrams*. Springer-Verlag, New York, N.Y.

COATS, C.J.A. & SNAJDR, P. (1984): Ore deposits of the North Range, Onaping–Levack area. *In* The Geology and Ore Deposits of the Sudbury Structure (E.G. Pye, A.J. Naldrett & P.E. Giblin, eds.). *Ontario Geol. Surv., Spec. Vol.* **1**, 327-346.

COWAN, J.C. (1968): Geology of the Strathcona ore deposit. *Can. Inst. Mining Metall., Bull.* **61**(699), 38-45.

DEER, W.A., HOWIE, R.A. & ZUSSMAN, J. (1972): *The Rock-Forming Minerals*. **2A**. *Chain Silicates*. John Wiley and Sons, New York, N.Y.

DIETZ, R.S. (1964): Sudbury structure as an astrobleme. *J. Geol.* **72**, 412-434.

DRESSLER, B.O. (1984): The effects of the Sudbury event and the intrusion of the Sudbury Igneous Complex on the footwall rocks of the Sudbury structure. *In* The Geology and Ore Deposits of the Sudbury Structure (E.G. Pye, A.J. Naldrett & P.E. Giblin, eds.). *Ontario Geol. Surv., Spec. Vol.* **1**, 97-136.

FARROW, C.E.G. (1995): *Geology, Alteration, and the Role of Fluids in Cu–Ni–PGE Mineralization of the Footwall Rocks to the Sudbury Igneous Complex, Levack and Morgan Townships, Sudbury District, Ontario*. Ph.D. thesis, Carleton University, Ottawa, Ontario.

_____ & WATKINSON, D.H. (1992): Alteration and the role of fluids in Ni,Cu, and platinum-group element deposition, Sudbury Igneous Complex contact, Onaping–Levack area, Ontario. *Mineral. Petrol.* **46**, 67-83.

_____ & _____ (1999): An evaluation of the role of fluids in Ni–Cu–PGE-bearing, mafic-ultramafic systems: dynamic processes in magmatic ore deposits and their application to mineral exploration. *Geol. Assoc. Can., Short Course Notes* **13**, 31-67.

FEDOROWICH, J.S., ROUSELL, D.H. & PEREDERY, W.V. (1999): Sudbury Breccia distribution and orientation in an embayment environment. *Geol. Soc. Am., Spec. Pap.* **339**, 305-315.

FRAPE, S.K. & FRITZ, P. (1987): Geochemical trends from groundwaters from the Canadian Shield: saline water and gases in crystalline rocks. *In* Saline Water and Gases in Crystalline Rocks (P. Fritz & S.K. Frape, eds.). *Geol. Assoc. Can., Spec. Pap.* **33**, 19-38.

FRY, N. (1984): *The Field Description of Metamorphic Rocks*. John Wiley & Sons, London, U.K.

GRIEVE, R.A.F. (1994): An impact model of the Sudbury Structure. *In* Proc. Sudbury–Noril'sk Symposium (P.C. Lightfoot & A.J. Naldrett, eds.). *Ontario Geol. Surv., Spec. Vol.* **5**, 119-132.

HANLEY, J.J. (2002): *The Distribution of the Halogens in Sudbury Breccia Matrix as Pathfinder Elements for Footwall Cu–PGE Mineralization at the Fraser Cu Zone, Barnet Main Copper Zone, and Surrounding Margin of the Sudbury Igneous Complex, Onaping–Levack Area, Ontario, Canada*. M.Sc. thesis, Univ. Toronto, Toronto, Ontario.

JAGO, B.C., MORRISON, G.G. & LITTLE, T.L. (1994): Metal zonation patterns and microtextural and micromineralogical evidence for alkali- and halogen-rich fluids in the genesis of the Victor Deep and McCreedy East footwall copper ore bodies, Sudbury Igneous Complex. *In* Proc. Sudbury–Noril'sk Symposium (P.C. Lightfoot & A.J. Naldrett, eds.). *Ontario Geol. Surv., Spec. Vol.* **5**, 65–75.

JOBSTRAIBIZER, P.G. & DE PIERI, R. (1984): Crystal chemistry of amphiboles from gabbroic to granodioritic rock types of the Adamello Massif (northern Italy). *Rend. Soc. Ital. Mineral. Petrol.* **39**, 123-144.

KORMOS, S.E. (1999): *Metal Distribution Within Zone 39, A Proterozoic Vein-Type Cu–Ni–Au–Ag–PGE Deposit, Strathcona Mine, Ontario, Canada*. M.Sc. thesis, Laurentian Univ., Sudbury, Ontario.

KROGH, T.E., DAVIS, D.W. & CORFU, F. (1984): Precise U–Pb zircon and baddeleyite ages for the Sudbury area. *In* The Geology and Ore Deposits of the Sudbury Structure (E.G. Pye, A.J. Naldrett & P.E. Giblin, eds.). *Ontario Geol. Surv., Spec. Vol.* **1**, 431-446.

LEAKE, B.E., chairperson (1997): Nomenclature of amphiboles: report of the Subcommittee on Amphiboles of the International Mineralogical Association, Commission on New Minerals and Mineral Names. *Can. Mineral.* **35**, 219-246.

LI, CHUSI (1992): *A Quantitative Model for the Formation of Sulfide Ores at Sudbury and a Study on the Distributions of Platinum-Group Elements in the Strathcona Copper-Rich Zones, Sudbury, Ontario*. Ph.D. thesis, Univ. of Toronto, Toronto, Ontario.

_____ & NALDRETT, A.J. (1993): High chlorine alteration minerals and calcium-rich brines in fluid inclusions from the Strathcona deep copper zone, Sudbury, Ontario. *Econ. Geol.* **88**, 1780-1796.

LIOU, J.G., KUNIYOSHI, S. & ITO, K. (1974): Experimental studies of the phase relations between greenschist and amphibolite in a basaltic system. *Am. J. Sci.* **274**, 613-632.

MARSHALL, D., WATKINSON, D., FARROW, C., MOLNAR, F. & FOUILLAC, A.-M. (1999): Multiple fluid generations in the Sudbury igneous complex: fluid inclusion, Ar, O, H, Rb and Sr evidence. *Chem. Geol*. **154**, 1–19.

MCCORMICK, K.A., LESHER, C.M., MCDONALD, A.M., FEDOROWICH, J.S. & JAMES, R.S. (2002): Chlorine and alkali geochemical halos in the Footwall Breccia and sublayer norite at the margin of the Strathcona Embayment, Sudbury Structure, Ontario. *Econ. Geol.* **97**, 1509-1519.

_____ & MCDONALD, A.M. (1999): Chlorine-bearing amphiboles from the Fraser mine, Sudbury, Ontario, Canada: description and crystal chemistry. *Can. Mineral.* **37**, 1385-1403.

MOODY, J.D., MEYER, D. & JENKINS, J.E. (1983): Experimental characterization of the greenschist/amphibolite boundary in mafic systems. *Am. J. Sci.* **283**, 48-92.

MOLNAR, F., WATKINSON, D.H. & JONES, P.C. (2001): Multiple hydrothermal processes in footwall units of the North Range, Sudbury igneous complex, Canada, and implications for the genesis of vein-type Cu–Ni–PGE deposits. *Econ. Geol*. **96**, 1645-1670.

MORRISON, G.G., JAGO, B.C. & WHITE, T.L. (1994): Footwall mineralization of the Sudbury Igneous Complex. *In* Proc. Sudbury–Noril'sk Symposium (P.C. Lightfoot & A.J. Naldrett, eds.). *Ontario Geol. Surv., Spec. Vol.* **5**, 57–64.

MORRISON, J. (1991): Compositional constraints on the incorporation of Cl into amphiboles. *Am. Mineral*. **76**, 1929-1930.

MUNOZ, J.L. (1984): F–OH and Cl–OH exchange in micas with applications to hydrothermal ore deposits. *In* Micas (S.W. Bailey, ed.). *Rev. Mineral*. **13**, 469-493.

_____ & LUDINGTON, S. (1977): Fluorine–hydroxyl exchange in synthetic muscovite and its application to muscovite–biotite assemblages. *Am. Mineral.* **62**, 304-308.

OBERTI, R., UNGARETTI, L., CANNILLO, E. & HAWTHORNE, F.C. (1993): The mechanism of Cl incorporation in amphibole. *Am. Mineral.* **78**, 746-752.

RAMBERG, H. (1952)**:** Chemical bonds and the distribution of cations in silicates. *J. Geol.* **60**, 331-355.

ROBINSON, O., SPEAR, F.S., SCHUMACHER, J.C., LAIRD, J., KLEIN, C., EVANS, B.W. & DOOLAN, B.L. (1982): Phase relations of metamorphic amphiboles: natural occurrence and theory. *In* Amphiboles: Petrology and Experimental Phase Relations (D.R. Veblen & P.H. Ribbe, eds.). *Rev. Mineral*. **9B**, 1-227.

ROSENBERG, P.E. & FOIT, F.F., JR. (1977): Fe^{2+}–F avoidance in silicates. *Geochim. Cosmochim. Acta* **41**, 345-346.

SHAND, S.J. (1916): The pseudotachylite of Parijs (Orange Free State). *Geol. Soc. London, Quart. J*. **72**, 198-221.

SKINNER, B.J., WHITE, D.E., ROSE, H.J., JR. & MAYS, R.E. (1967): Sulfides associated with the Salton Sea geothermal brine. *Econ. Geol*. **62**, 316-330.

SPRAY, J.G. (1997): Superfaults. *Geology* **25**, 579-582.

SPEAR, F.S. (1981): An experimental study of hornblende stability and compositional variability in amphibolite. *Am. J. Sci*. **281**, 697-734.

SPRINGER, G. (1989): Chlorine-bearing and other uncommon minerals in the Strathcona Deep Copper zone, Sudbury District, Ontario. *Can. Mineral.* **27**, 311-313.

VOLFINGER, M., ROBERT, J.-L., VIELZEUF, D. & NEIVA, A.M.R. (1985): Structural control of the chlorine content of OH-bearing silicates (micas and amphiboles). *Geochim. Cosmochim. Acta* **49**, 37- 48.

WILSHIRE, H.G. (1971): Pseudotachylites from the Vredefort Ring, South Africa. *J. Geol.* **79**, 195-206.

WINKLER, H.G.F. (1967): *Die Genese der metamorphen Gesteine* (second ed.). Springer-Verlag, Berlin, Germany.

YARDLEY, B.W.D. (1989): *An Introduction to Metamorphic Petrology*. Longman Group, Essex, U.K.

ZHU, CHEN & SVERJENSKY, D.A. (1991): Partitioning of F–Cl–OH between minerals and hydrothermal fluids. *Geochim. Cosmochim. Acta* **55**,1837-1858.

_____ & _____ (1992): F–Cl–OH partitioning between biotite and apatite. *Geochim. Cosmochim. Acta* **56**, 3435-3467.

Received November 8, 2002, revised manuscript accepted June 10, 2003.